Disrupted PI3K subunit p110α signaling protects against pulmonary hypertension and reverses established disease in rodents

Eva M. Berghausen,[1,2,3] Wiebke Janssen,[4,5] Marius Vantler,[1,2,3] Leoni L. Gnatzy-Feik,[1,2,3] Max Krause,[1,2,3] Arnica Behringer,[1,2] Christine Joseph,[1,2] Mario Zierden,[1,2,3] Henrik ten Freyhaus,[1,2,3] Anna Klinke,[1,2,3] Stephan Baldus,[1,2,3] Miguel A. Alcazar,[2,6,7] Rajkumar Savai,[4] Soni Savai Pullamsetti,[4] Dickson W.L. Wong,[8] Peter Boor,[8] Jean J. Zhao,[9] Ralph T. Schermuly,[4,5] and Stephan Rosenkranz[1,2,3]

[1]Department of Cardiology, Heart Center at the University of Cologne, Cologne, Germany. [2]Center for Molecular Medicine Cologne (CMMC) and [3]Cologne Cardiovascular Research Center (CCRC), University of Cologne, Cologne, Germany. [4]Max-Planck Institute for Heart and Lung Research, Bad Nauheim, Germany. [5]University of Giessen and Marburg Lung Center (UGMLC), and German Centre for Lung Research (DZL), Giessen, Germany. [6]Institute for Lung Health, member of the DZL, UGMLC, Giessen, Germany. [7]Department of Pediatric and Adolecent Medicine, University of Cologne, Cologne, Germany. [8]Institute of Pathology, RWTH Aachen University Hospital, Aachen, Germany. [9]Dana-Farber Cancer Center, Harvard Medical School, Boston, Massachusetts, USA.

Enhanced signaling via RTKs in pulmonary hypertension (PH) impedes current treatment options because it perpetuates proliferation and apoptosis resistance of pulmonary arterial smooth muscle cells (PASMCs). Here, we demonstrated hyperphosphorylation of multiple RTKs in diseased human vessels and increased activation of their common downstream effector phosphatidylinositol 3′-kinase (PI3K), which thus emerged as an attractive therapeutic target. Systematic characterization of class IA catalytic PI3K isoforms identified p110α as the key regulator of pathogenic signaling pathways and PASMC responses (proliferation, migration, survival) downstream of multiple RTKs. Smooth muscle cell–specific genetic ablation or pharmacological inhibition of p110α prevented onset and progression of pulmonary hypertension (PH) as well as right heart hypertrophy in vivo and even reversed established vascular remodeling and PH in various animal models. These effects were attributable to both inhibition of vascular proliferation and induction of apoptosis. Since this pathway is abundantly activated in human disease, p110α represents a central target in PH.

Introduction

Pulmonary hypertension (PH) is a frequent phenomenon, which is characterized by limited treatment options and high mortality (1). PH may occur as a consequence of left heart disease, chronic lung disease, thromboembolic disease, or as a distinct disorder of the pulmonary arterioles. Pulmonary arterial hypertension (PAH), representing group 1 of the clinical PH classification (2), is the best-characterized entity among the various forms of PH. Functional and structural abnormalities of pulmonary resistance vessels contribute to PAH onset and progression, resulting in progressive pulmonary vascular remodeling (3–5). Consequently, there is a constant rise in pulmonary artery pressure and pulmonary vascular resistance, which represent a sustained increase of right ventricular afterload, eventually leading to right heart failure and death (6–8).

Despite recent improvements, the morbidity and mortality of PAH remain unacceptably high, with annual mortality rates at approximately 3% to 20% (9–11), so improved treatment strategies are urgently needed. Current therapies mainly aim to restore the imbalance of mediators regulating vascular tone, and recent approaches focus on antiproliferative strategies, aiming at preventing or even reversing pathological vascular remodeling. Peptide growth factors, which elicit their signals via RTKs, play a prominent role in this process. For instance, studies reporting expression analyses, genetic modifications, or pharmacological interventions suggest a role for PDGF in experimental and human PH (12–16). Indeed, the tyrosine kinase inhibitor (TKI) imatinib, which targets the Bcr/Abl oncogene *c-kit* and PDGFR, was sufficient to reverse pulmonary vascular remodeling and PH in experimental models (13), and it improved exercise capacity and hemodynamics in patients with severe PAH in a randomized placebo-controlled trial (16). However, this was accompanied by severe adverse events, and only a subset of patients responded to this therapy (17).

The latter may be explained by the fact that other growth factors, such as EGF, insulin, IGF-I, and basic FGF (bFGF), are also involved in the pathobiology of PAH (18–22) and provide a proproliferative and antiapoptotic environment such that inhibition of PDGF signaling alone may not be efficient. One way to overcome this problem is to target a common downstream mediator of multiple RTKs. Utilizing chimeric CSF1R/βPDGFR mutants, we recently identified phosphatidylinositol 3′-kinase (PI3K) as the critical βPDGFR-associated signaling molecule mediating mitogenic responses in vascular smooth muscle cells (SMCs) in the context of neointima formation (23) and PH (14).

Conflict of interest: The authors have declared that no conflict of interest exists.

Submitted: February 3, 2020; **Accepted:** August 18, 2021; **Published:** October 1, 2021.
Reference information: *J Clin Invest*. 2021;131(19):e136939.
https://doi.org/10.1172/JCI136939.

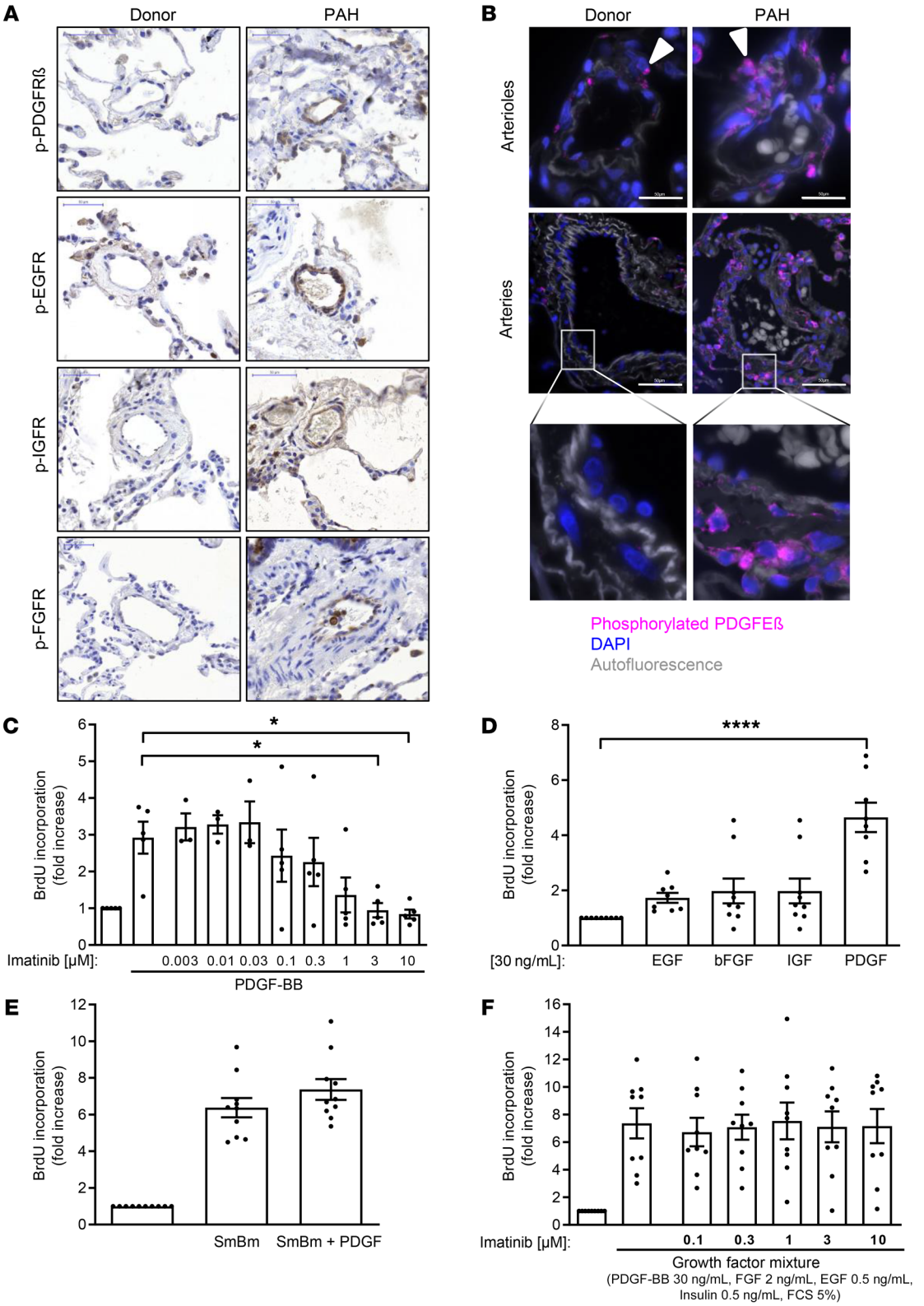

Figure 1. Multiple growth factors contribute to PAH and hPASMC proliferation. (**A**) Representative immunohistochemical staining showing phosphorylation of the indicated RTKs in lung tissue from healthy donors and patients with idiopathic PAH ($n = 4$ each). Scale bar: 50 µm. (**B**) Immunofluorescent staining demonstrating phosphorylation of PDGFβ receptor in the media of pulmonary arteries/arterioles from patients with PAH ($n = 4$; for control staining, see Supplemental Figure 1). Scale bar: 50 µm. (**C**–**F**) Proliferative response (BrdU incorporation) of hPASMCs to various growth factors and inhibition by the tyrosine kinase inhibitor imatinib. Quiescent cells were stimulated with either PDGF-BB (**C**), various growth factors as indicated (**D**), smooth muscle basal medium (SmBm: FGF [2 ng/mL], EGF [0.5 ng/mL], insulin [0.5 µg/mL], FCS [5%]) alone or with PDGF-BB (30 ng/mL), subsequently referred to as growth factor mixture (GFM) (**E**), and GFM (**F**), as indicated. In **C** and **F**, cells were preincubated with the indicated concentrations of imatinib for 30 minutes. Data were normalized to starved controls and represent mean ± SEM. $^*P < 0.05$; $^{****}P < 0.0001$ as assessed by 1-way ANOVA with Dunnett's test ($n = 7$–10 in each group).

PI3Ks are lipid kinases generating 3-phosphoinositides, which are capable of transmitting various intracellular signals. According to their structural characteristics and substrate specificity, PI3Ks are divided into 3 main classes, of which class IA PI3Ks act downstream of RTKs (24–26). They consist of a regulatory p85 subunit and 1 of 3 distinct 110-kDa catalytic subunits (p110α, p110β, p110δ), catalyzing the phosphorylation of phosphatidyinositol-4,5-bisphosphate (PIP_2) to the second messenger phosphatidyinositol-3,4,5-trisphosphate (PIP_3). PIP_3 serves as a docking site for downstream signaling molecules such as AKT, which is considered the major transducer of PI3K signal relay (27). Since broad-spectrum PI3K inhibition is expected to be poorly tolerated, the targeted inhibition of a selective catalytic class IA PI3K isoform, which acts as a common RTK downstream transducer and converges their signals (24–26), appears as an attractive therapeutic strategy.

Here, we provide evidence that among the catalytic PI3K isoforms, p110α is the key downstream mediator of mitogenic, chemotactic, and antiapoptotic signaling by multiple RTKs, and thus represents a central contributor to the hyperproliferative and apoptosis-resistant phenotype of pulmonary arterial smooth muscle cells (PASMCs). Utilizing a genetic and a pharmacological approach, we demonstrated that selective disruption of p110α signaling in PASMCs blunted pathogenic signaling and PASMC responses in vitro and was highly effective in preventing or even reversing pulmonary vascular remodeling, PH, and right heart hypertrophy in several PH animal models in vivo. Since this pathway is abundantly activated in human PAH, we present a potentially novel therapeutic concept focusing on this central downstream mediator.

Results

Multiple growth factors contribute to human PAH and PASMC proliferation. When monitoring the role of peptide growth factors in human PAH, we found several RTKs, including PDGFR, EGFR, IGFR, and FGFR, in a phosphorylated and thus activated state in remodeled vessels (Figure 1A), particularly in the medial layer (Figure 1B). PASMCs as opposed to endothelial cells appeared as the most relevant cell type in this context (Supplemental Figure 2A; supplemental material available online with this article; https://doi.org/10.1172/JCI136939DS1). In isolated human PASMCs (hPASMCs), PDGF — representing the most potent mitogen among the tested growth factors — but also EGF, bFGF, and IGF exhibited a marked proliferative response (Figure 1, C and D and Supplemental Figure 2B). The TKI imatinib, which inhibits the PDGFR, expectedly inhibited PDGF-dependent hPASMC proliferation in a concentration-dependent manner (Figure 1C). However, it is crucial to evaluate the inhibitory potency of a compound under conditions that better reflect the in vivo situation in diseased tissue. To this end, we established optimized growth conditions by combining smooth muscle growth medium (SmGm), which contains various growth factors (FGF, EGF, insulin, FCS), with additional PDGF-BB (Supplemental Figure 2C). This growth factor mixture (GFM) led to a robust increase of BrdU incorporation to 7.4-fold the basal level (Figure 1E). This approach better mimics the pathophysiological conditions in PAH lungs, as it comprises a combination of relevant growth factors instead of a single growth factor. Importantly, and in contrast to PDGF-stimulated cells, imatinib was no longer able to sufficiently suppress mitogenesis when the cells were stimulated with GFM (Figure 1F).

PI3K/AKT signaling is enhanced in human and experimental PH. Based on the established role of PI3K/AKT downstream of RTKs, we hypothesized that inhibition of this pathway enables hindering of pathogenic cellular responses induced by multiple growth factors. Indeed, in contrast to imatinib, the pan PI3K inhibitor LY294002 led to a concentration-dependent reduction in PDGF- and GFM-induced proliferation and chemotaxis of hPASMCs and AKT phosphorylation, respectively (Figure 2, A–F). Importantly, analysis of lung homogenates from patients with idiopathic PAH (IPAH) compared with healthy donors revealed markedly enhanced AKT phosphorylation in vivo (Figure 2G), and lung tissue from mice with hypoxia-induced PH also displayed elevated levels of phosphorylated AKT when compared with normoxic controls (Figure 2H). Immunostaining of human lung tissue samples revealed that AKT phosphorylation was particularly enhanced in the remodeled vascular wall in IPAH (Figure 2I). Collectively, our data demonstrated that PI3K is crucial for growth factor–induced responses in hPASMCs, and PI3K activity was profoundly enhanced in remodeled vessels in human and experimental PH.

Catalytic PI3K subunit p110α is essential for growth factor–mediated cellular responses of hPASMCs. Since broad-spectrum PI3K inhibition is expected to be associated with potential toxicity, we aimed to identify the distinct function of each of the catalytic class IA isoforms (p110α, p110β, and p110δ) for growth factor–dependent PASMC responses. Expression analyses revealed that all 3 isoforms were present in hPASMCs (Figure 3A) and demonstrated similar mRNA and protein levels in lung tissue and isolated PASMCs from patients with IPAH compared with healthy donors, indicating that p110 isoforms were not upregulated in diseased tissue (Figure 3, B–D). However, abundant phosphorylation of p110α-activating RTKs and its downstream target AKT at the site of vascular remodeling indicate increased p110 signaling in PH in vivo.

In order to systematically investigate the impact of each of the catalytic class IA PI3K subunits, we utilized isoform-specific small molecule inhibitors of p110α (PIK75), p110β (TGX221), and p110δ (IC87114). Inhibition of p110α led to a concentration-dependent reduction in PDGF- and GFM-dependent proliferation and chemotaxis of hPASMCs, whereas inhibition of p110β and p110δ did not affect these responses (Figure 3, E–H). Consistently, proliferation induced by single application of EGF, IGF, or bFGF was also reduced by PIK75 but not TGX221 or IC87114 (Supplemental Figure 3). In line with these findings, inhibition of p110α — but not p110β or p110δ — potently restrained GFM-induced AKT phosphorylation (Figure 3I), and PIK75 also abrogated mitogenic signaling events downstream of AKT, such as phosphorylation of GSK3β, FoxO, induction of cyclin D1, and phosphorylation of the retinoblastoma protein (Rb) (Figure 3J). Additionally, GFM-dependent protection against apoptosis was reversed by p110α inhibition (Figure 3K). Of note, the antimitogenic and proapoptotic effects of p110α inhibition were also found in diseased hPASMCs isolated from patients with IPAH (Figure 3, L and M).

Lack of p110α in PASMCs attenuates growth factor–induced responses. Based on the above findings, we hypothesized that p110α plays a central role in the pathobiology of PH. However, a potential concern with the use of pharmacological inhibitors is their specificity. In order to confirm the crucial role of p110α for PASMC responses and PH in vivo, we therefore aimed to assess its role by means

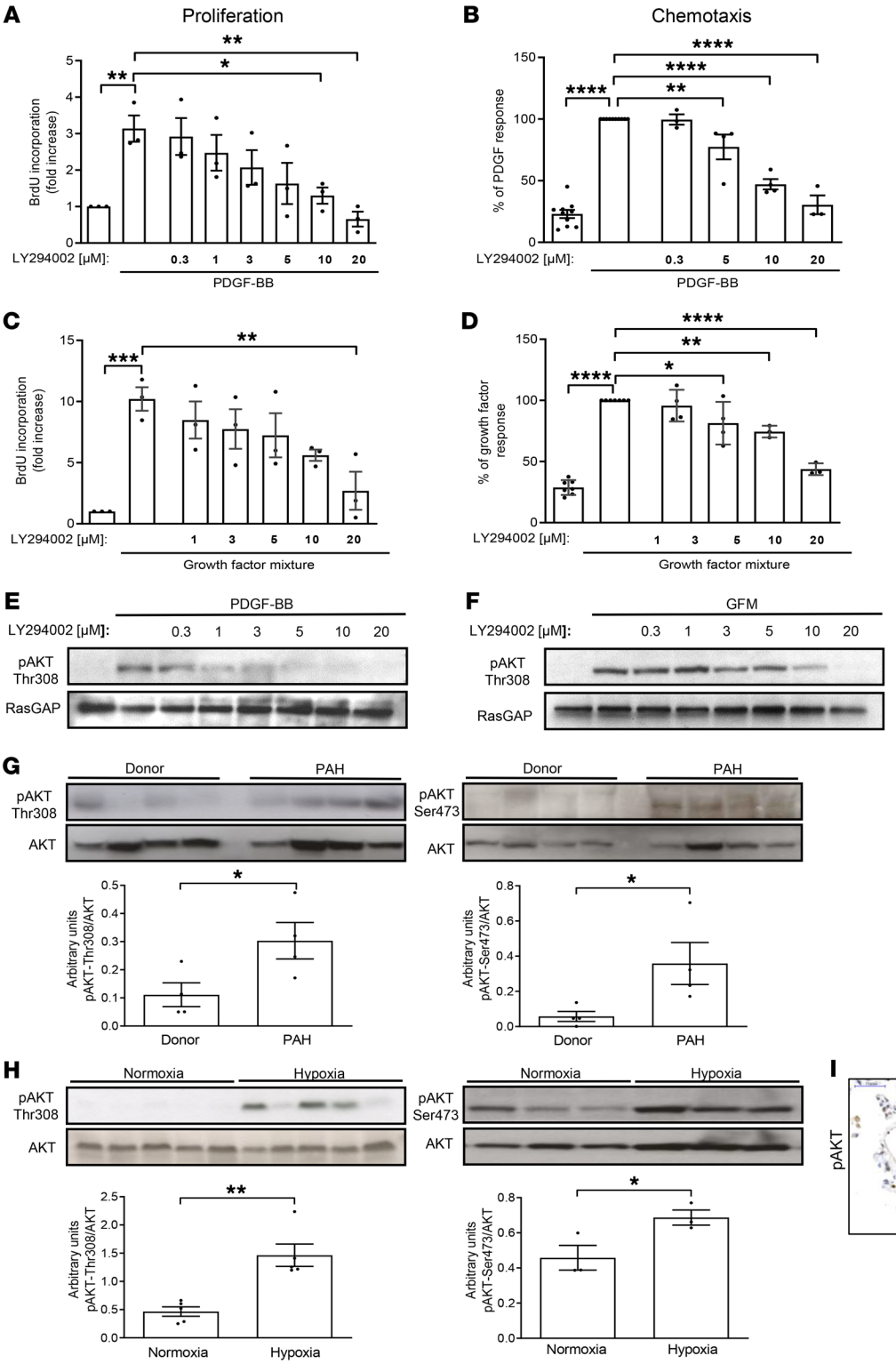

Figure 2. PI3K signaling is enhanced in PAH and contributes to hPASMC proliferation. (**A** and **B**) PDGF-BB–dependent (30 ng/mL) proliferation (**A**) (determined by BrdU incorporation; $n = 3$ each) and chemotaxis (**B**) (assessed by modified Boyden chambers; $n = 10, 10, 3, 4, 4, 3$) of hPASMCs in the presence of indicated concentrations of the pan-PI3K inhibitor LY294002. (**C** and **D**) Growth factor mixture–induced (GFM-induced) proliferation ($n = 3$ each) and chemotaxis ($n = 7, 7, 4, 4, 3, 3$) in the presence of indicated concentrations of the pan-PI3K inhibitor LY294002. (**E** and **F**) PDGF-BB–induced (30 ng/mL) and GFM-induced phosphorylation of AKT (Thr308) in LY294002 preincubated hPASMCs ($n = 3$). (**G** and **H**) AKT phosphorylation (Thr308 and Ser473) in lung tissue homogenates from patients with IPAH versus healthy donors ($n = 4$ each) and (**G**) in hypoxia-exposed mice and normoxic controls ($n = 5$, 5 and 3, 3) (**H**). RasGAP or total AKT is shown as loading control, and quantification was performed by densitometric analysis. Results are shown as pAKT/AKT ratio. In all quantitative analyses, data represent mean ± SEM. $^{*}P < 0.05$; $^{**}P < 0.01$; $^{***}P < 0.001$; $^{****}P < 0.0001$ as assessed by (**A**–**D**) 1-way ANOVA with Dunnett's test and (**G**–**H**) Student's 2-tailed t test. (**I**) Immunohistochemical staining demonstrating enhanced AKT phosphorylation in lung tissue from patients with IPAH versus healthy donors (400-fold magnification; $n = 4$). Scale bar: 50 μm.

of a genetic model. Since whole-body p110α knockout mice or mice expressing a kinase-inactive p110α mutant ($p110\alpha^{D933A/D933A}$) are not viable (28), a smooth muscle–specific p110α-deficient mouse model (sm-$p110\alpha^{-/-}$) was generated (29, 30). These mice were viable and did not display an obvious phenotype under basal conditions (30). SM-specific p110α deficiency was proven via protein expression analysis in homogenates from the pulmonary artery, which correlated with a profound reduction of basal AKT phosphorylation in vivo (Figure 4A). Decreased levels of p110α were also found in the aorta, whereas p110α expression remained unaltered in the liver, thus confirming tissue specificity of the model (Supplemental Figure 4, A and B). Absence of p110α protein in PASMCs was confirmed in cell lysates from sm-$p110\alpha^{-/-}$ mice (Figure 4B), p110β and p110δ expression remained unaltered, and

p85 was slightly reduced. Of note, p110α$^{+/-}$ and p110α$^{-/-}$ PASMCs displayed reduced mitogenesis in tissue culture as compared with WT cells under basal conditions (Supplemental Figure 4C).

Consistent with the above results utilizing small molecule inhibitors, p110α$^{-/-}$ PASMCs were not able to efficiently proliferate or migrate upon stimulation with either PDGF-BB or GFM (Figure 4, C–F). Likewise, AKT phosphorylation was reduced in p110α$^{+/-}$ and even further diminished in p110α$^{-/-}$ cells (Figure 4G), and p110α deficiency abundantly attenuated further downstream signaling events, such as phosphorylation of GSK3β, FoxO, and Rb, as well as cyclin D1 expression (Figure 4H and Supplemental Figure 5). These experiments also revealed that PIK75 did not further inhibit signaling events in PASMCs from sm-p110α$^{-/-}$ mice. Moreover, p110α$^{-/-}$ mouse PASMCs (mPASMCs) displayed a significantly higher apoptosis rate upon serum deprivation as compared with p110α$^{+/+}$ cells, and this could not be rescued by PDGF-BB (Figure 4I). In summary, the above results indicate that p110α plays a central role in PASMC proliferation, migration, and apoptosis induced by multiple growth factors.

SM-specific p110α deficiency and pharmacological inhibition of p110α prevent hypoxia-induced vascular remodeling and PH in vivo. To evaluate the role of p110α for the onset and progression of PH in vivo, WT, sm-p110α$^{+/-}$, and sm-p110α$^{-/-}$ mice were subjected to the PH model of chronic hypoxia. As expected, hypoxia augmented vascular muscularization in small pulmonary arteries (<70 μm) of WT mice, as indicated by a significant decrease of nonmuscularized vessels paralleled by an increase of the portion of partially and fully muscularized vessels (Figure 5, A and B). Likewise, medial wall thickness of small pulmonary vessels (<50 μm) from hypoxia-exposed WT animals was significantly enhanced (Figure 5C). The hypoxia-induced increase in both muscularization and medial wall thickness was almost completely abrogated in sm-p110α$^{-/-}$ mice when compared with WT littermates (Figure 5, A–C).

Under normoxic conditions, no differences in right ventricular systolic pressure (RVSP) were detected among the different genotypes. As expected, chronic hypoxia led to a significant increase of RVSP in WT mice (34.9 ± 1.1 mmHg), which was less pronounced in sm-p110α$^{+/-}$ mice (32.5 ± 0.6 mmHg) and significantly lower (31.1 ± 1.5 mmHg) in sm-p110α$^{-/-}$mice. In contrast, systemic systolic blood pressure (SBP) was similar among the 6 groups (Figure 5E). As a consequence of increased right ventricle (RV) afterload, hypoxia-challenged WT mice displayed RV hypertrophy expressed as the ratio of RV weight to left ventricular (LV) weight inclusive of the septum (RV/LV + S) (0.38 ± 0.03), whereas there was no significant increase in sm-p110α$^{+/-}$ (0.32 ± 0.03) and sm-p110α$^{-/-}$ (0.32 ± 0.01) mice (Figure 5F), indicating that sm-specific p110α deficiency was protective against PH-related RV hypertrophy.

We next assessed whether pharmacological inhibition of p110α is also sufficient to prevent hypoxia-induced PH. To this end, WT mice were treated with the p110α inhibitor PIK75 or vehicle during hypoxia exposure. Figure 5, G–I demonstrate that treatment with PIK75 was able to prevent vascular remodeling, in that both hypoxia-induced muscularization and medial wall thickening were significantly reduced in PIK75-treated animals. In addition, the hypoxia-induced increase in RVSP was significantly lowered by PIK75, and RV hypertrophy was prevented without any effects on systemic hemodynamics (Figure 5, J–L). In sm-specific p110α-deficient and PIK75-treated mice, enhanced AKT phosphorylation in lung tissue upon hypoxia exposure was reduced compared with WT or vehicle treatment (Supplemental Figure 6, A and B).

Therapeutic p110α inhibition reverses established pulmonary vascular remodeling and PH in rats. The above data showed that p110α deficiency/inhibition was able to prevent hypoxia-induced PH in mice, so we next examined the effects of p110α inhibition on established PH, which is more comparable to the situation when the disease is diagnosed in humans. To this end, we utilized the models of Sugen/hypoxia-induced (Su/Hx-induced) or monocrotaline-induced (MCT-induced) severe PH in rats. In the Su/Hx model, which best resembles the pulmonary vascular lesions observed in human PAH (31, 32), rats were injected with SU5416 followed by 3 weeks of hypoxia. Subsequently, treatment with PIK75 or vehicle was started at day 21 and maintained for 14 days until analysis and harvesting (Figure 6A). Su/Hx rats displayed substantial morphological changes in pulmonary vessels: both the degree of muscularization and medial wall thickness of small vessels (<50 μm) were profoundly increased in vehicle-treated animals (Figure 6, B–D). This was accompanied by a significant increase of RVSP (27.3 ± 0.7 vs. 81.1 ± 9.8 mmHg) and RV hypertrophy (RV/LV + S 0.29 ± 0.017 vs. 0.53 ± 0.04; Figure 6, E and F). Pulmonary vascular remodeling, the increase in RVSP, and RV hypertrophy were all reversed by PIK75 therapy and almost reached the values observed in healthy animals (RVSP 41.2 ± 3.9; RV/LV + S 0.37 ± 0.02; Figure 6, C–F). No effects on SBP or heart rate were noticed (Supplemental Figure 7, A and B). Reversed remodeling in PIK75-treated animals was attributable to a decrease in the number of proliferating (proliferating cell nuclear antigen–positive [PCNA-positive]) vascular cells and an increase in the number of apoptotic (TUNEL-positive) cells (Figure 6, G and H) in conjunction with increased caspase 9 (Supplemental Figure 7C). Furthermore, increased AKT phosphorylation in the lungs of Su/Hx rats was reduced in PIK75-treated animals (Supplemental Figure 6C). Similar findings were obtained in a second therapeutic approach in the MCT model of established PH (Supplemental Figure 8, A–G).

Finally, we tested a second compound inhibiting p110α (BYL719) for its ability to suppress experimental PH. In the hypoxia mouse model, BYL719 was applied at a concentration of 50 mg/kg/d and significantly attenuated pulmonary vascular remodeling, RVSP, and RV hypertrophy (RV/LV + S; Figure 7, A–E). Likewise, BYL719 (20 mg/kg/d) was also able to reverse established PH in Su/Hx-exposed rats (Figure 7, F–J). These experiments confirmed that inhibition of p110α by BYL719 nearly normalized the number of PCNA-positive cells, predominantly in the medial layer of the vessel wall (Figure 7K). Consistently, BYL719 attenuated growth factor–induced cellular responses in isolated hPASMCs and mPASMCs (Supplemental Figures 9 and 10).

Hence, pharmacological inhibition of p110α by 2 distinct compounds (PIK75, BYL719) was able to reverse pulmonary vascular abnormalities, PH, and RV hypertrophy in various animal models in vivo.

Discussion

Herein, we systematically analyzed the contribution of catalytic class IA PI3K isoforms acting downstream of multiple RTKs to cellular responses of PASMCs in vitro and to pathogenic vascu-

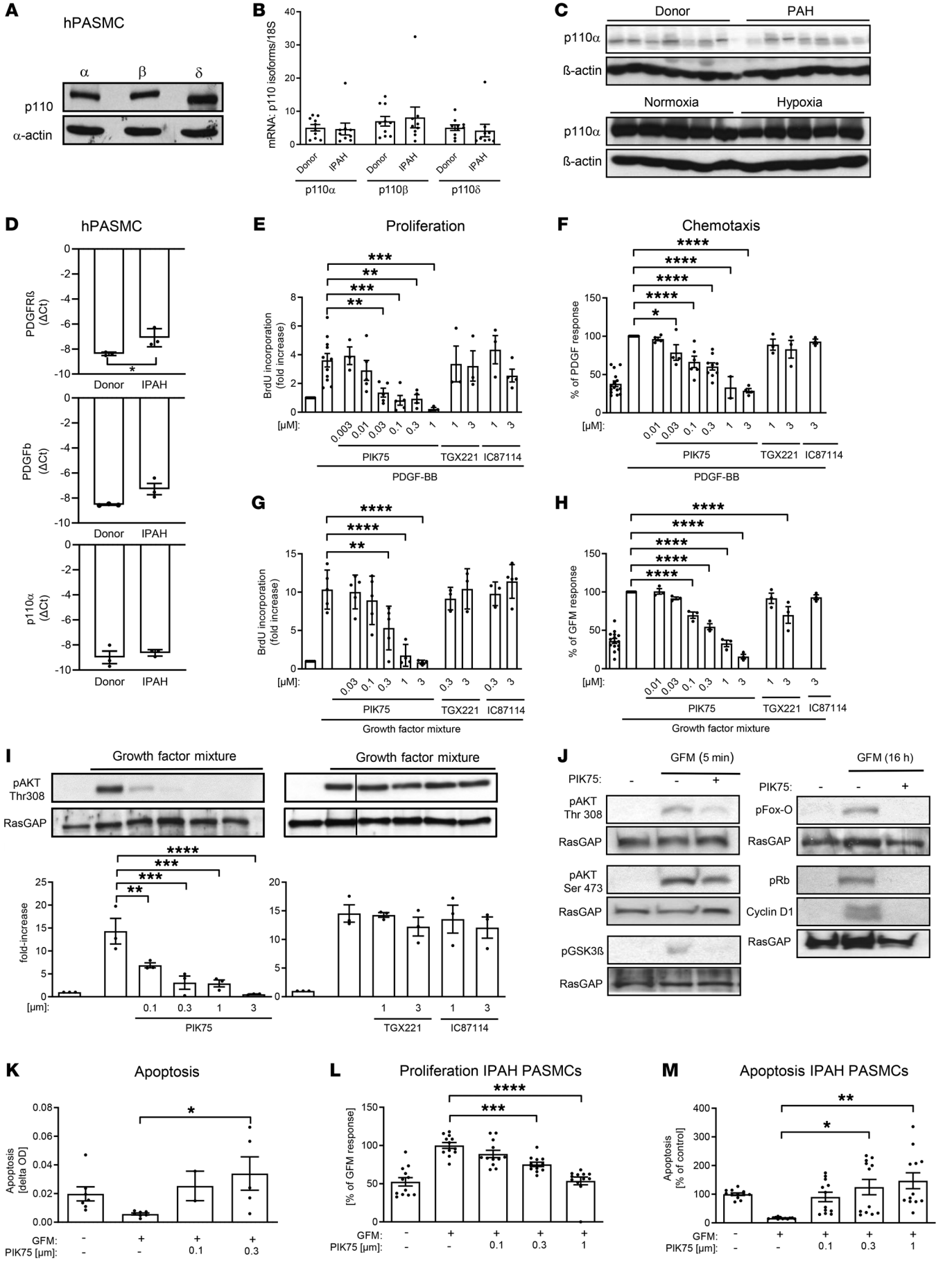
A
hPASMC
α β δ
p110
α-actin
B
mRNA: p110 isoforms/18S
Donor IPAH Donor IPAH Donor IPAH
p110α p110β p110δ
C
Donor PAH
p110α
ß-actin
Normoxia Hypoxia
p110α
ß-actin
D
hPASMC
PDGFRß (ΔCt)
PDGFb (ΔCt)
p110α (ΔCt)
Donor IPAH
E
Proliferation
BrdU incorporation (fold increase)
[μM]:
PIK75
TGX221
IC87114
PDGF-BB
F
Chemotaxis
% of PDGF response
[μM]:
PIK75
TGX221
IC87114
PDGF-BB
G
BrdU incorporation (fold increase)
[μM]:
PIK75
TGX221
IC87114
Growth factor mixture
H
% of GFM response
[μM]:
PIK75
TGX221
IC87114
Growth factor mixture
I
Growth factor mixture
Growth factor mixture
pAKT Thr308
RasGAP
fold-increase
[μm]:
PIK75
TGX221
IC87114
J
GFM (5 min)
GFM (16 h)
PIK75:
pAKT Thr 308
RasGAP
pAKT Ser 473
RasGAP
pGSK3ß
RasGAP
pFox-O
RasGAP
pRb
Cyclin D1
RasGAP
K
Apoptosis
Apoptosis [delta OD]
GFM:
PIK75 [μm]:
L
Proliferation IPAH PASMCs
[% of GFM response]
GFM:
PIK75 [μm]:
M
Apoptosis IPAH PASMCs
Apoptosis [% of control]
GFM:
PIK75 [μm]:

Figure 3. The class IA PI3K isoform p110α mediates growth factor–dependent responses in PASMCs. (**A**) Western blot analysis demonstrating the expression of the catalytic class IA PI3K subunits in hPASMCs. Blots were probed with isoform-specific p110 antibodies; α-actin shown as a loading control (3 repetitions). (**B**) Expression of p110 subunits in human lung tissue from healthy donors and patients with IPAH (n = 9 each). Shown is the ratio of p110 mRNA to the internal control (18S) as assessed by TaqMan probes. (**C**) p110α expression in human (upper; n = 7 each) and mouse lung tissue (lower; n = 5 each). (**D**) Real-time PCR demonstrating the mRNA expression of PDGFRβ (upper), PDGF-B (middle), and p110α (lower) in PASMCs from healthy donors or patients with IPAH (n = 3 each). (**E** and **F**) PDGF-BB–dependent (30 ng/mL) proliferation (**E**) (BrdU-incorporation; n = 11, 11, 3, 5, 5, 5, 3, 3, 3, 3, 4) and chemotaxis (**F**) (modified Boyden chambers; n = 15, 15, 4, 4, 6, 9, 2, 4, 3, 3, 3) of hPASMCs in the presence of PI3K isoform-specific inhibitors of p110α (PIK75), p110β (TGX221), and p110δ (IC87114) in the indicated concentrations. (**G** and **H**) Proliferation (n = 5, 5, 5, 5, 5, 4, 4, 3, 3, 3, 4) (**F**) and chemotaxis (n = 15, 15, 3, 3, 3, 3, 3, 3, 3, 3, 3) (**H**) of GFM-stimulated hPASMCs in the absence or presence of PI3K inhibitors. (**I**) Impact of PI3K inhibitors against p110α (left) and p110β or p110δ (right) on GFM-induced AKT phosphorylation (Thr 308) in PASMCs (n = 3 each). RasGAP shown as loading control and quantification performed by densitometric analysis. Data shown as fold-increase normalized to quiescent controls. (**J**) Downstream signaling in hPASMCs preincubated with PIK75 (300 nM) and stimulated with GFM for either 5 minutes (top) or 16 hours (bottom). RasGAP shown as loading control. (**K**) Apoptosis of starved (24 hours) hPASMCs stimulated with GFM in absence or presence of PIK75 (0.1 and 0.3 μM) (n = 7, 7, 2, 5). (**L** and **M**) Proliferation (n = 12) and apoptosis (n = 12) of hPASMCs from patients with PAH stimulated with GFM in absence or presence of PIK75 (at indicated concentrations). Data expressed as percentage of quiescent control (apoptosis) or GFM (proliferation). Data in **D**–**I** and **K**–**M** represent mean ± SEM. $^{*}P < 0.05$; $^{**}P < 0.01$; $^{***}P < 0.001$; $^{****}P < 0.0001$ as assessed by (**E**–**I** and **K**–**M**) 1-way ANOVA with Dunnett's test and (**D**) 2-tailed Student's t test.

lar remodeling and PH in vivo. The data presented are consistent with the schematic diagram outlined in Figure 8 and allow 4 important conclusions: (a) the PI3K/Akt pathway was active in human and experimental PH and mediated pathogenic cellular responses in PASMCs downstream of multiple RTKs; (b) among the catalytic class IA PI3K isoforms, p110α was critically involved in pulmonary vascular remodeling as assessed by genetic and pharmacological approaches; (c) downstream consequences of p110α signaling resembled typical features of PAH, i.e., a proproliferative and apoptosis-resistant PASMC phenotype; and (d) disruption of p110α signaling was sufficient to prevent and reverse pathogenic pulmonary vascular remodeling, PH, and consecutive RV hypertrophy in 4 distinct disease models in vivo. Since this pathway is abundantly activated in human disease, p110α appears as a central target in PH.

Our findings are of clinical relevance since there is an urgent need to further improve morbidity and mortality in PH (9–11, 33), and there is proof of concept for antiremodeling strategies in humans given that inhibition of RTK signaling by imatinib was efficacious at least in a subset of patients when applied in addition to established PAH therapies (15, 16). However, safety concerns preclude its routine clinical use, and imatinib was not efficient in all patients. The data presented herein provide a molecular explanation for the latter. Since we and others found multiple RTKs to be activated and relevant in PAH (12–14, 18–22), it is likely that the contribution of single growth factors that trigger vascular remodeling is variable among individual patients. In fact, the disease may be mainly driven by PDGF in some patients, whereas signals initiated by other growth factors may be predominant in others. Hence, we postulated that targeting a common central signaling event downstream of multiple RTKs — such as p110α — would represent a logical and efficient treatment approach.

In order to prove the role of p110α independently from pharmacological inhibitors, which may lack specificity, we established a genetic model of smooth muscle–specific p110α deficiency. In PASMCs lacking p110α, no compensatory regulation of other p110 isoforms was detected. As expected, expression of p85 was slightly diminished, since it is known to form obligate heterodimers with p110 (34, 35). PDGF- and GFM-induced AKT activity and proliferation and chemotaxis of PASMCs were decreased in heterozygous p110α-deficient cells and nearly completely abrogated in homozygous p110α knockout cells. Furthermore, lack of proper p110α signaling also diminished critical downstream events such as phosphorylation of GSK3β, cyclin D1 induction, and Rb phosphorylation. Unphosphorylated Rb prevents cell cycle progression by directly binding to and inhibiting transcription factors (36). FoxO transcription factors are key regulators of cellular proliferation and apoptosis (37–39), which are also regulated in PH (40). Nuclear exclusion of FoxO enhances transcription of cyclins and reduces transcription of the CDK inhibitor $p27^{Kip1}$ (39, 41, 42). In our setting, phosphorylation of FoxO1 at threonine 24 and FoxO3a at threonine 32 were enhanced upon GFM stimulation in WT cells causing its nuclear exclusion, whereas in cells lacking p110α their phosphorylation was largely diminished. Hence, defective p110α signaling prevented the subcellular events promoting mitogenesis as well as apoptosis in mPASMCs and hPASMCs.

The postulated crucial role of PI3K/AKT signaling in the pathobiology of PAH is further supported by studies demonstrating that sm-specific depletion of the phosphatase and tensin homolog (PTEN), which antagonizes class I PI3K signaling, leads to medial hyperplasia and vascular remodeling through increased proliferation of SMCs (43), which is associated with spontaneous development of RV hypertrophy under normoxic conditions and a profound PH phenotype under hypoxia (44). Conversely, PTEN overexpression and deficiency of Akt1 and inducible SM-specific depletion of mTOR protected against hypoxia-induced PH (45), and targeted deletion of the antiproliferative transcription factor FoxO1 in SMCs resulted in exaggerated PH (40). In line with this concept, the expression of PTEN was downregulated in experimental PH (46), and increased levels of phosphorylated (inactive) PTEN (44) as well as downregulation and inactivation of FoxO1 (40) were found in human PAH lungs. Collectively, these data are consistent with our analyses of lung tissue from patients with PAH as well as mice exposed to hypoxia, demonstrating that the PI3K/AKT pathway is highly activated. Profoundly increased levels of phosphorylated AKT were particularly found in remodeled vessels, where growth factors and RTKs are upregulated (12–14, 18–22). Hence, PI3K/AKT signaling is closely linked to the vascular abnormalities in PH.

In our in vivo models, both genetic ablation and pharmacological inhibition of p110α nearly completely abrogated remodeling of the small pulmonary arteries and largely prevented the development of PH. The choice to target p110α was based on a system-

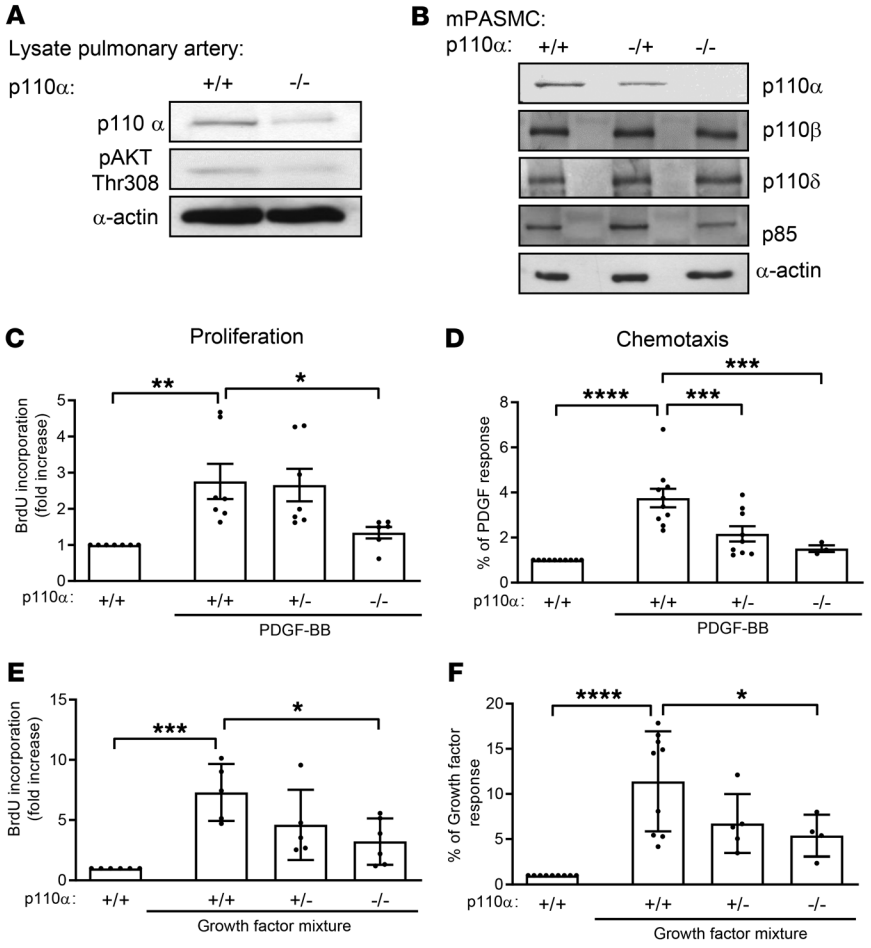

Figure 4. Lack of p110α in smooth muscle cells attenuates growth factor–induced responses. (**A**) Expression of p110α and phosphorylation of AKT (Thr308) in pulmonary arteries from smooth muscle–specific p110α-deficient mice (sm-p110α$^{-/-}$) compared with WT control mice (sm-p110α$^{+/+}$) (3 repetitions). (**B**) Expression of the 3 catalytic class IA PI3K p110 subunits and the regulatory p85 subunit in murine PASMCs isolated from sm-p110α$^{+/+}$, sm-p110α$^{+/-}$, or sm-p110α$^{-/-}$ mice; α-actin shown as loading control (3 repetitions). (**C**–**F**) PDGF-BB–induced (n = 7 each) or growth factor mixture–induced (GFM-induced) proliferation (BrdU incorporation) (n = 5 each) and chemotaxis as indicated in PASMCs isolated from sm-p110α$^{+/+}$, sm-p110α$^{+/-}$, or sm-p110α$^{-/-}$ mice (n = 10, 10, 10, 3 and n = 9, 9, 4, 4). (**G**) Effects of hetero- and homozygous p110α deficiency on PDGF-BB (30 ng/mL) or GFM-dependent AKT (Thr308) phosphorylation in mPASMCs. RasGAP shown as a loading control. (**H**) Downstream signaling in mPASMCs isolated from WT (sm-p110α$^{+/+}$) or homozygous p110α-deficient mice (sm-p110α$^{-/-}$) left untreated or preincubated with PIK75 (300 nM) and stimulated with GFM for either 5 minutes (top panel) or 16 hours (bottom panel). RasGAP shown as loading control. Note that in contrast to WT cells stimulated with either PDGF or GFM, PIK75 did not further affect downstream signaling events in p110α-deficient PASMCs, indicating that PIK75 at the indicated concentration of 1 μM specifically inhibited p110α. (**I**) Apoptosis of serum-starved and PDGF-BB–treated mPASMCs isolated from sm-p110α$^{+/+}$ or sm-p110α$^{-/-}$ mice (n = 5 each). All data (**C**–**F** and **I**) represent mean ± SEM, $^{*}P < 0.05$; $^{**}P < 0.01$; $^{***}P < 0.001$; $^{****}P < 0.0001$ as assessed by 1-way ANOVA with Dunnett's test.

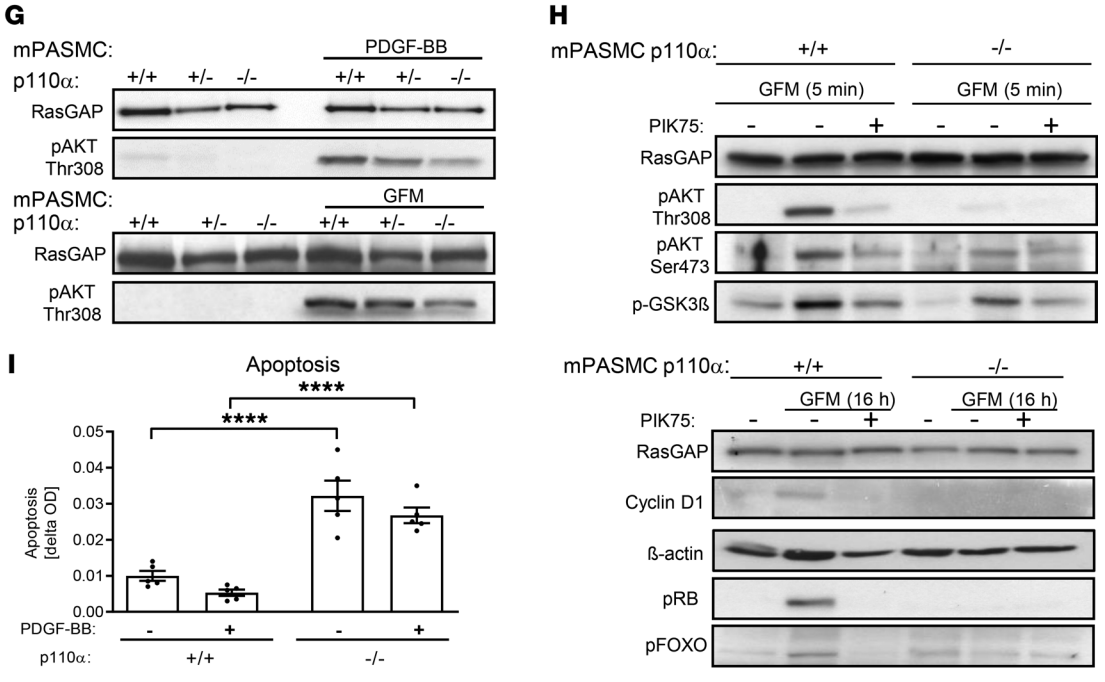

atic approach characterizing the role of class IA PI3K isoforms in PASMCs by the use of isoform-specific inhibitors, where only p110α inhibition — and subsequently its targeted deletion — were able to abrogate growth factor–dependent abnormalities in proliferation, migration, and apoptosis. Thus, interference with p110α signaling was able to fully reverse the features of PH in vitro and in vivo. The relevance of this pathway in the context of PH is further supported by our previous findings, that RTK signaling and the progression

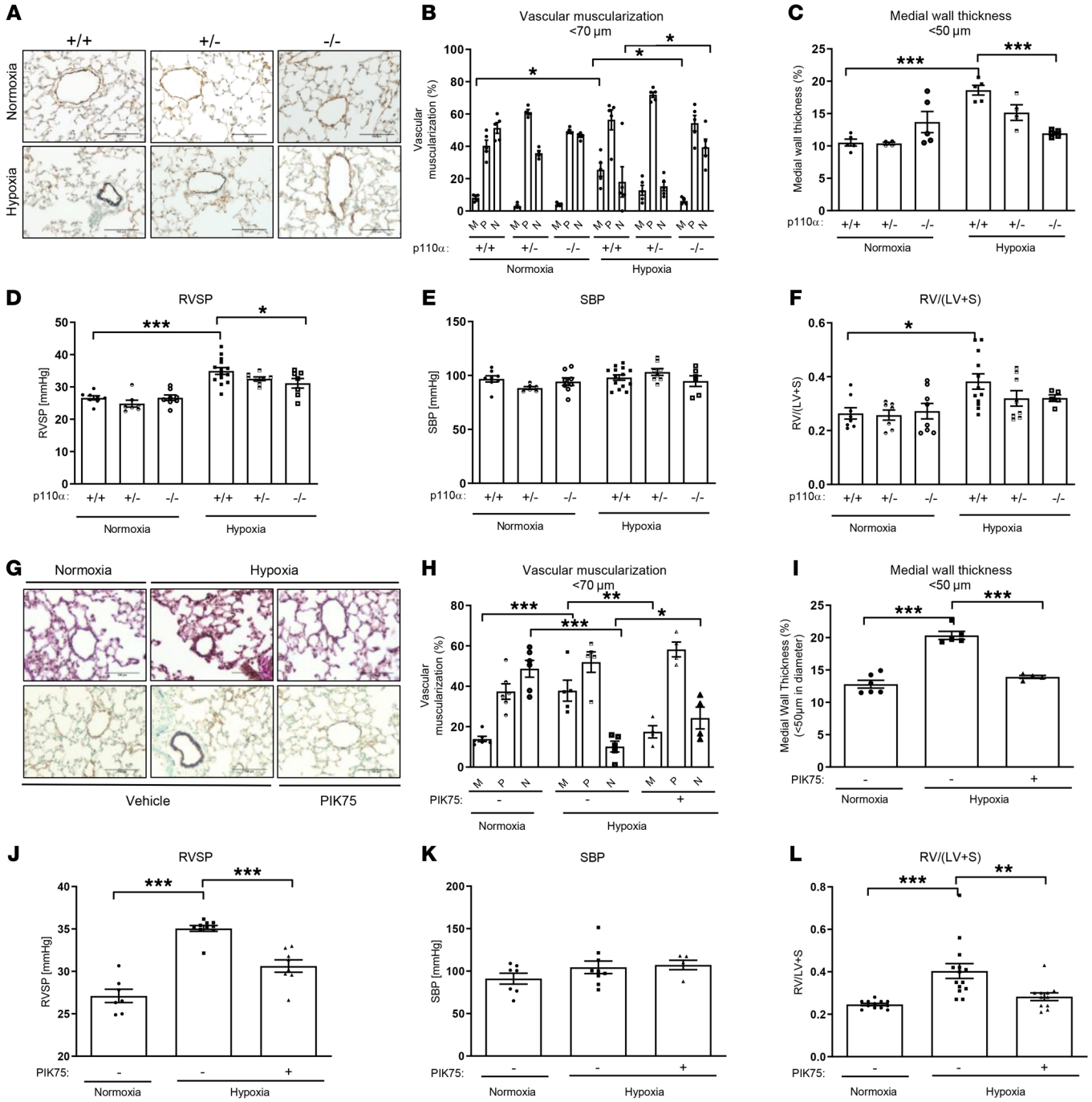

Figure 5. SM-specific p110α deficiency and pharmacological inhibition of p110α prevent hypoxia-induced pulmonary hypertension. (**A**) Representative immunostainings of small pulmonary arteries from sm-p110α$^{+/+}$, sm-p110α$^{-/+}$, and sm-p110α$^{-/-}$ mice exposed to normoxia or hypoxia (10% O_2 for 21 days). Shown are representative images of lung sections immunostained for vWF (brown) and α-smooth muscle actin (purple), 400-fold magnification. Scale bar: 100 μm. (**B**) Quantitative morphometric analysis of muscularization of small (<70 μm) pulmonary vessels from the above animals. Shown is the percentage of fully (M), partially (P), and nonmuscularized (N) vessels (at least 80 analyzed per animal), *n* = 5, 4, 5, 5, 5, 5. (**C**) Quantitative assessment of medial wall thickness of small (<50 μm) pulmonary arteries from the above animals (*n* = 5, 4, 5, 5, 4, 5). (**D**) RVSP (mmHg), measured by a Millar microtip catheter (1F) inserted into the right ventricle via the jugular vein, *n* = 8, 7, 8, 14, 8, 7. (**E**) SBP (mmHg) was measured using a Millar microtip catheter (1F) inserted into the left carotid artery, *n* = 8, 6, 8, 14, 8, 6. (**F**) RV hypertrophy is shown as RV/LV + S ratio, *n* = 8, 7, 8, 12, 8, 5. (**G**–**L**) Pulmonary vascular remodeling and pulmonary hemodynamics of PIK75-treated WT mice exposed to hypoxia. (**G**) Representative images of Van Gieson staining demonstrating the medial wall thickness (upper panel) and double-immunostaining for vWF and α-smooth muscle actin demonstrating the muscularization (lower panel) of peripheral pulmonary arteries. Scale bar: 100 μm. (**H**) Impact of p110α inhibition with PIK75 on vascular muscularization of small (<70 μm) pulmonary arteries, *n* = 6, 5, 4 and (**I**) medial wall thickness of less than 50 μm pulmonary arteries, *n* = 6, 5, 4. (**J**) Impact of p110α inhibition with PIK75 on RVSP, *n* = 7, 10, 8; (**K**) SBP, *n* = 7, 9, 5, and (**L**) RV hypertrophy, expressed as the RV/LV + S ratio; *n* = 12, 14, 11. All data represent mean ± SEM. **P* < 0.05; ***P* < 0.01; ****P* < 0.001 as assessed by ANOVA followed by a Newman-Keuls post hoc test.

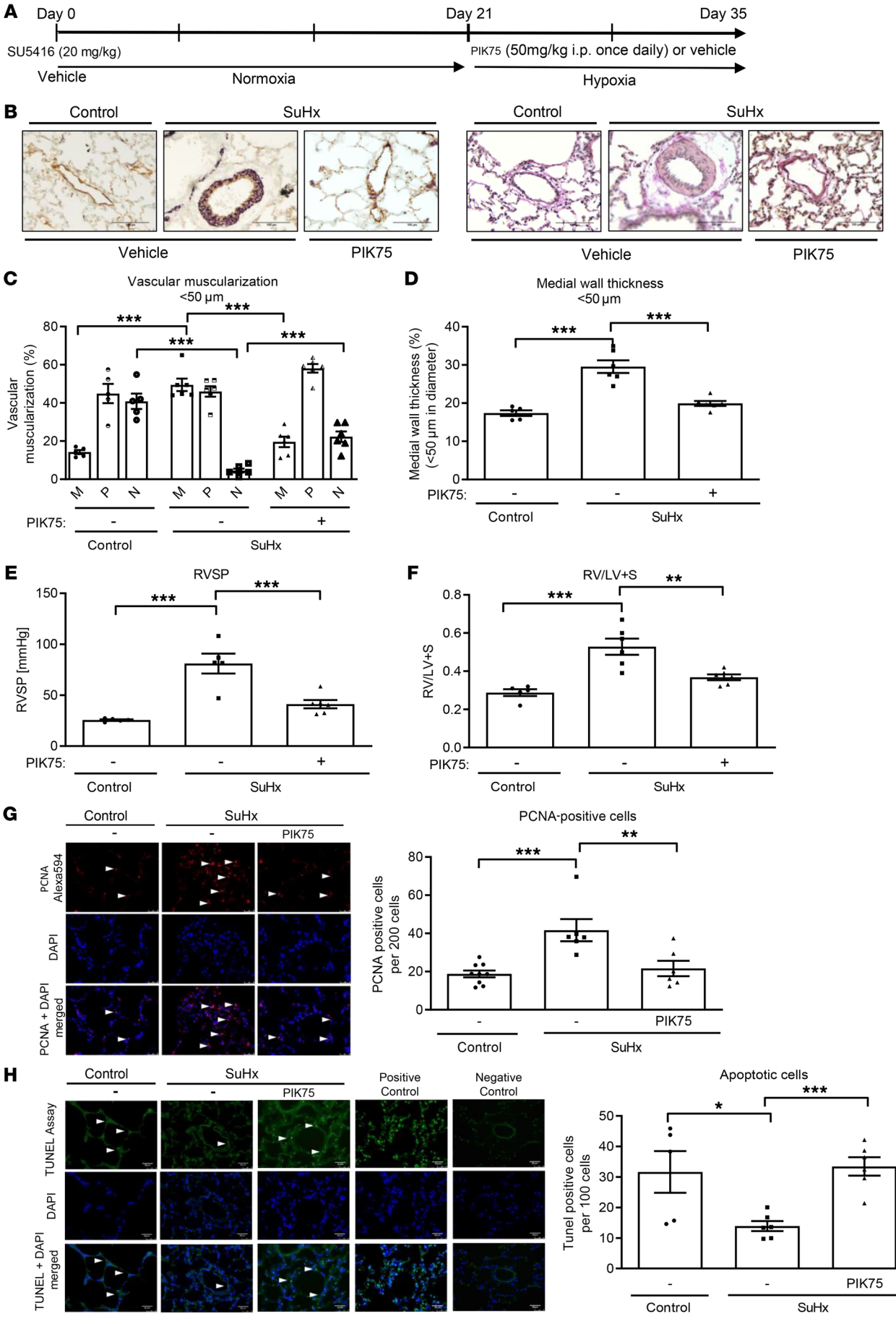
A
Day 0
Day 21
Day 35
SU5416 (20 mg/kg)
Vehicle
Normoxia
PIK75 (50mg/kg i.p. once daily) or vehicle
Hypoxia
B
Control
SuHx
Vehicle
PIK75
C
Vascular muscularization <50 µm
Vascular muscularization (%)
M P N
PIK75:
Control
SuHx
D
Medial wall thickness <50 µm
Medial wall thickness (%) (<50 µm in diameter)
E
RVSP
RVSP [mmHg]
F
RV/LV+S
G
PCNA Alexa594
DAPI
PCNA + DAPI merged
PCNA-positive cells
PCNA positive cells per 200 cells
H
TUNEL Assay
TUNEL + DAPI merged
Positive Control
Negative Control
Apoptotic cells
Tunel positive cells per 100 cells

Figure 6. Therapeutic inhibition of p110α reverses Su/Hx-induced pulmonary hypertension. (**A**) Schematic diagram illustrating the treatment protocol in the Su/Hx model. (**B**) Double-immunostaining for vWF (brown) and α-smooth muscle actin (purple) demonstrating the muscularization (left panel) of peripheral pulmonary arteries or Van Gieson staining demonstrating medial wall thickness (right panel) in control animals versus untreated or PIK75-treated Su/Hx-induced pulmonary hypertension. Shown are representative images of lung sections. Scale bar: 100 μm. (**C**) Impact of p110α inhibition with PIK75 on vascular muscularization of small pulmonary arteries (<50 μm) from animals as indicated. Shown is the percentage of fully (M), partially (P), and nonmuscularized (N) vessels (at least 80 were analyzed per animal), n = 5, 6, 6. (**D**) Medial wall thickness of less than 50 μm pulmonary arteries, n = 5, 6, 6; (**E**) RVSP (mmHg), n = 5, 5, 6; (**F**) RV hypertrophy expressed as RV/LV + S ratio, n = 5, 6, 6. (**G**) Representative immunofluorescence photo-micrographs of PCNA (red) and DAPI (blue) in small pulmonary vessels from rats (scale bar: 20 μm, arrowheads indicate PCNA-positive cells) (left panel) and quantification of proliferating cells (right panel). Shown are PCNA-positive cells per total cells from 10 representative vessels, randomized to 200 cells, n = 9, 6, 6. (**H**) Immunofluorescence staining of TUNEL (green) and DAPI (blue) in small pulmonary vessels (scale bar: 20 μm, arrowheads indicate TUNEL-positive cells) (left panel) and quantification of apoptotic cells (right panel). Shown are TUNEL-positive cells per total cells from 10 representative vessels, randomized to 100 cells, n = 5, 6, 6. All data represent mean ± SEM. $^*P < 0.05$; $^{**}P < 0.01$; $^{***}P < 0.001$ as assessed by ANOVA followed by a Newman-Keuls post hoc test.

of PH are even enhanced under hypoxic conditions via HIF1α-dependent downregulation of RTK-antagonizing protein-tyrosine phosphatases (47), and p110α deficiency also prevented neointima formation after balloon angioplasty (30). Of major importance is the fact that p110α inhibition was effective in established PH and the in vitro findings were corroborated in diseased human PAH cells. Because the majority of patients with PAH display severe pulmonary vascular alterations at the time of diagnosis, therapeutic approaches that can reverse remodeling are highly warranted when treatment is initiated. Here, therapeutic application of the p110α inhibitors PIK75 and BYL719 markedly improved hemodynamics and RV hypertrophy in the Su/Hx rat model of PH, which is characterized by severe obstructive vascular lesions and best reflects the vascular abnormalities in human PAH (31, 32), although treatment was started when the disease had fully developed. This was confirmed in a second animal model (MCT-induced PH) and accompanied by a profound reduction of arteriolar muscularization and medial hypertrophy in both models, indicating reversal of pulmonary vascular remodeling, which was linked to antiproliferative and proapoptotic effects. Although we observed a substantial therapeutic effect on vascular morphology and pulmonary hemodynamics in both the Su/Hx and MCT models of established PH, the full efficacy profile of pharmacological p110α inhibition may not have been captured because we applied only a single concentration of PIK75 and BYL719, and assessments of hemodynamics and RV morphology were performed at only one time point.

A concern with systemic inhibition of p110α by a pharmacological compound is tolerability or potential toxicity. Previous studies reported impairments in glucose and insulin tolerance by p110α inhibition in animals and humans. Furthermore, cardiac-specific ablation of p110α was associated with decreased cardiac contractility (48), potentially due to dysregulation of L-type Ca^{2+} channels (49). Additionally, it was shown that constitutively active p110α, in contrast to dominant-negative p110α was associated with preserved cardiac contractility after myocardial infarction, indicating a potential importance for maintaining cardiac function in settings of cardiac stress (50). On the other hand, PIK75 did not cause heart failure in our models, and selective PI3K inhibitors appear to be well tolerated in humans when tested for cancer (51, 52). Besides the potential side effects of pharmacological agents inhibiting p110α, a potential caveat with the genetic model is that in addition to the impact of sm-specific deficiency or haploinsufficiency of p110α on pulmonary vascular remodeling, the impact of the Cre transgene on cardiac hypertrophy and contractility cannot be ruled out (53). In addition, the specific strain of Tagln/SM22-Cre may cause unexpected recombination in myofibroblast and megakaryocyte populations (53), which could confound the phenotype.

Investigation of long-term altered p110α signaling revealed that a cardiac-specific dominant-negative p110α prevents cardiac aging in mice by preventing accumulation of lipofuscin, accompanied by increased autophagy and decreased oxidative stress (54). Additionally, chronic partial p110α inactivation (p110α D933/WT) prevented age-related reduction in insulin sensitivity and glucose tolerance, resulting in an extended lifespan in male mice (55). Together, these findings indicate the potential of undesirable short-term side effects of therapeutic p110α inhibition, such as impaired glucose tolerance, which was not observed in our model, however (see Supplemental Figure 11). Conversely, long-term inhibition may even lead to beneficial effects through metabolic adaptation (55). Still, potential systemic toxicity may be overcome by site-specific delivery methods for the lung (i.e., inhalation), as recently shown with other compounds (40), including a pan-PI3K inhibitor in the context of lung fibrosis (56).

In summary, our data provide strong evidence that the PI3K/AKT pathway is critically involved in the pathobiology of PH, which remains an incurable, devastating disease. Using genetic and pharmacological approaches, we identified p110α as a central downstream effector of multiple RTKs that mediated mitogenic, motogenic, and antiapoptotic effects in PASMCs in the medial layer of small pulmonary arterioles. Targeting p110α prevented and even reversed all central features of PH, including vascular remodeling, which is not mitigated by current therapies. Since this pathway is abundantly activated in human disease, targeted inhibition of p110α offers a disease-modifying treatment approach, which is readily accessible by small molecule inhibitors and warrants further evaluation in clinical trials.

Methods

Overall study design

The objective of this study was to explore the role of the catalytic PI3K isoform p110α for PASMC function in pulmonary vascular remodeling and its impact for the pathobiology of PH. The project was designed under the assumption that p110α — via acting as a key downstream mediator of multiple RTKs — may represent a central target in PH. We used samples from patients with idiopathic PAH to demonstrate that multiple RTKs as well as the respective common downstream pathway were abundantly activated in vascular lesions displaying features of PAH compared with healthy controls. Further, we used a systematic approach to dissect the role of the various catalytic class IA PI3K isoforms in hPASMCs in vitro,

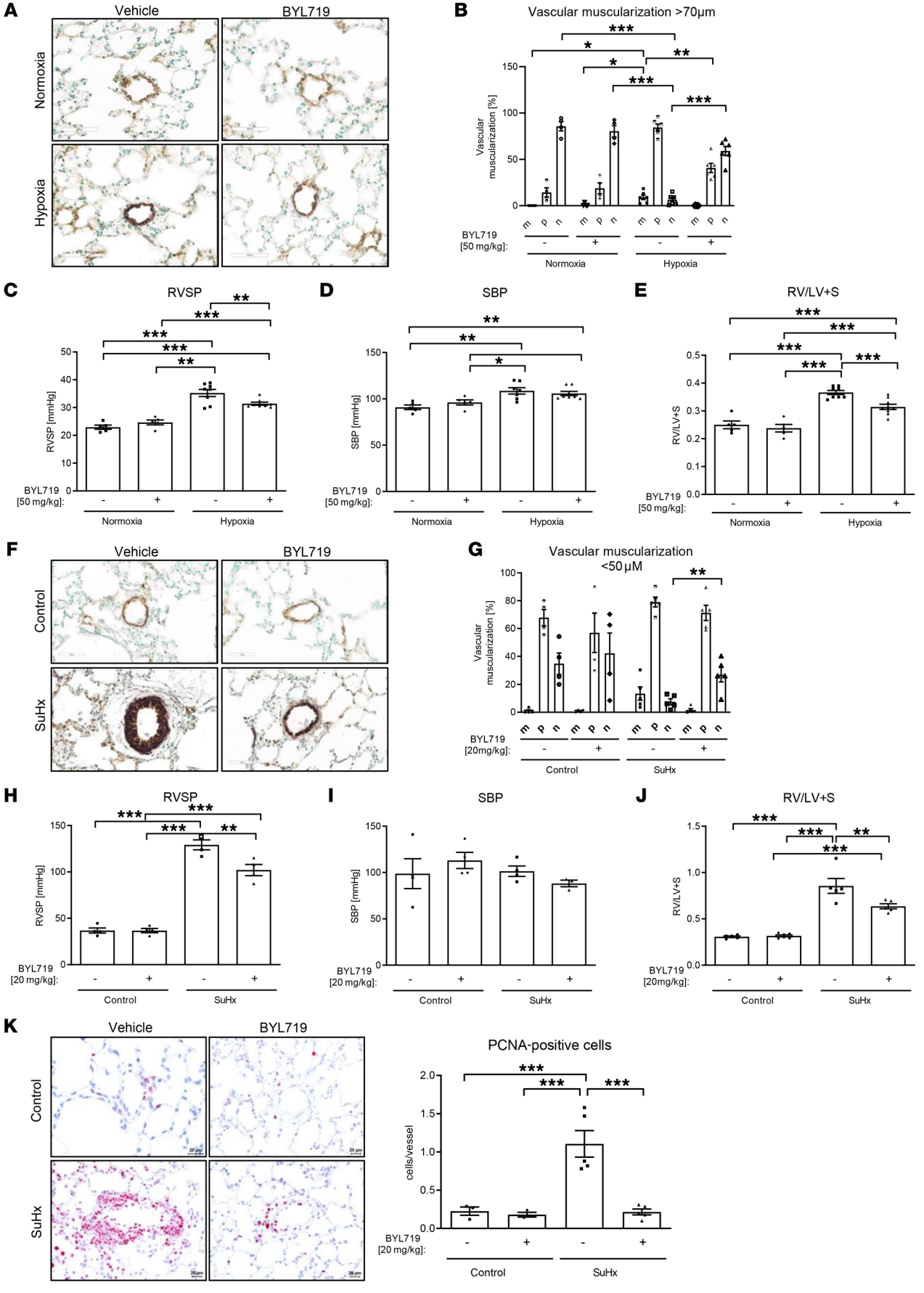
A
Vehicle
BYL719
Normoxia
Hypoxia
B
Vascular muscularization >70µm
Vascular muscularization [%]
BYL719 [50 mg/kg]:
Normoxia
Hypoxia
C
RVSP
RVSP [mmHg]
D
SBP
SBP [mmHg]
E
RV/LV+S
F
Control
SuHx
G
Vascular muscularization <50 µM
BYL719 [20mg/kg]:
H
I
J
K
PCNA-positive cells
cells/vessel

Figure 7. Inhibition of p110α using BYL719 impedes experimental pulmonary hypertension in mice and rats. (**A**) Representative images of a double-immunostaining for vWF (brown) and α-smooth muscle actin (purple) demonstrating the muscularization of peripheral pulmonary arteries. (**B**) Impact of p110α inhibition with BYL719 on vascular muscularization of small (<70 μm) pulmonary arteries. Shown is the percentage of fully (M), partially (P), and nonmuscularized (N) vessels Scale bar: 60 μm (n = 4, 4, 6, 6). Impact of BYL719 on (**C**) RVSP (mmHg) (n = 4, 4, 6, 6), (**D**) SBP (mmHg) (5, 5, 6, 8), and (**E**) RV hypertrophy (n = 5, 5, 8, 9), expressed as the RV/LV + S ratio. (**F**) Double-immunostaining for vWF and α-smooth muscle actin in control animals versus untreated or BYL719-treated animals with Su/Hx-induced pulmonary hypertension. Scale bar: 60 μm. (**G**) Impact of p110α inhibition with BYL719 on vascular muscularization of small pulmonary arteries (<50 μm) from animals as indicated (n = 4, 4, 5, 5) (**H**) RVSP (n = 4 each) (**I**) SBP (n = 4, 4, 4, 3), and (**J**) RV hypertrophy expressed as RV/LV + S ratio (n = 5, 6, 5, 5). (**K**) Representative immunohistochemical photomicrographs of PCNA (red) in small pulmonary vessels from rats (scale bar: 20 μm; left panel) and quantification of proliferating cells (right panel). Shown are PCNA-positive cells per vessel, (n = 3, 3, 5, 5). All data represent mean ± SEM. *P < 0.05; **P < 0.01; ***P < 0.001 as assessed by ANOVA followed by a Newman-Keuls post hoc test.

using isoform-specific small molecule inhibitors, as well as targeted gene deletion in mice. In vitro studies in human and murine cells included quantitative assessment of mitogenic (BrdU incorporation), chemotactic (modified Boyden chamber), and antiapoptotic (Cell Death Detection ELISA) signaling, as well as immunoblotting to monitor the expression levels or activation state of relevant downstream targets (e.g., Akt, GSK-3β, FoXO, pRB, cyclin D1). The in vitro experiments and data analysis were performed in an open-label manner.

To explore the contribution of p110α to pathogenic processes during PH development and progression in vivo, we used 3 distinct animal models of experimental PH to characterize pulmonary hemodynamics, pulmonary vascular morphometric analysis, and consecutive right heart hypertrophy in detail. We generated mice harboring a targeted gene deletion of p110α in SMCs (sm-p110$^{-/-}$) and subjected them to the hypoxia-induced mouse model of PH and applied a pharmacological approach by treating WT mice with isoform-specific p110α small molecule inhibitors (PIK75 or BYL719). In order to elaborate the therapeutic potential to reverse established disease, we utilized the Su/Hx and MCT rat models of PH. Animals were randomly assigned to experimental groups based on their age, body weight, and genotype. All investigators performing the experiments were blinded for the genotype or the treatment group of the respective animals during hemodynamic measurements and morphometric analysis of the lung tissue sections. Further mechanistic insights were obtained from immunoblotting, immunohistochemistry, and immunofluorescence staining. Details with regard to sampling and experimental replicates are provided in each figure legend.

Cells and cell culture

Human PASMCs (CC2581; lot 00003639143 [age: 43 years, sex: male, race: White] and lot 13981 [age: 2.5 months, sex: male, race: White]) were obtained from Lonza, and were maintained in Clonetics SmGm (CC3182). Mouse PASMCs were isolated from either WT, sm-p110α$^{+/-}$, or sm-p110α$^{-/-}$ mice by enzymatic dispersion as described (57). Briefly, mice were euthanized and the thorax dissected. The entire heart-lung complex was removed and placed in a culture dish filled with chilled PBS buffer supplemented with penicillin-streptomycin (1%). The pulmonary artery was carefully dissected, removed, and incubated in an enzyme solution of collagenase (Sigma-Aldrich), elastase (Serva Electrophoresis GmbH), and trypsin inhibitor (Sigma-Aldrich) for 15 minutes to detach the adventitia. The remaining adventitia was removed using anatomic forceps, and the endothelium was gently removed by scraping the luminal surface. The pure pulmonary artery was cut into smaller pieces and incubated for another 90 minutes at 37°C in the enzyme solution to disintegrate the tissue and separate the SMCs. After 2 minutes of centrifugation at 2000 rpm, the supernatant was discarded and the cell pellet was resuspended in DMEM culture medium containing 20% FCS and 1% penicillin/streptomycin. Cells were transferred into 24-well plates. After reaching 80% confluence, cells were expanded.

Cultured diseased PASMCs isolated from patients with PAH

Explant-derived PASMCs were obtained from human pulmonary arteries (<2 mm in diameter) isolated from patients with IPAH or from control donors and cultured as previously described (40). Patient characteristics are provided in Supplemental Methods.

Human tissue samples

Human lung tissue was obtained from either individuals with IPAH or healthy donors undergoing lung transplantation. Lung tissue was snap-frozen immediately after explantation.

Generation of smooth muscle–specific p110α-deficient mice

Smooth muscle–specific p110α knockout mice were generated by cross-breeding of homozygous PI3Kca$^{fl/fl}$ (p110α [lox/lox]) mice (29) with SM22-Cre mice (B6.Cg-Tg[Tagln-Cre]1Her/J, The Jackson Laboratory), which express Cre recombinase under the control of the mouse transgelin (smooth muscle protein 22-alpha) promoter. SM22-Cre$^{+/-}$/p110α$^{fl/+}$ mice were crossed to homozygous p110α$^{fl/fl}$ mice to generate SM22-Cre^{-}/p110α$^{fl/fl}$ (sm-p110α$^{+/+}$), SM22-Cre^{+}/p110α$^{fl/+}$ (sm-p110α$^{+/-}$), and SM22-Cre^{+}/p110α$^{fl/fl}$ (sm-p110α$^{-/-}$) littermates (30). Genotyping was performed by PCR using tail biopsies.

Animals and PH models

Hypoxia-induced PH. Male WT sm-p110α$^{+/-}$ or sm-p110α$^{-/-}$ mice (20–30 g, 8–16 weeks) were kept in a BioSpherix hypoxia chamber (10% normobaric oxygen) for 21 days. Treatment was carried out in C57BL/6J mice (JAX mice strain, Charles River Laboratories) by daily i.p. injection of 50 mg/kg PIK75 (suspended in 20% β-hydroxypropyl-cyclodextrin solution in saline buffer) or by oral gavage of 50 mg/kg BYL719 (suspended in 1% carboxymethyl cellulose).

MCT-induced PH. Male Sprague-Dawley rats (8 weeks old) (Charles River Laboratories, Janvier Labs) received a single s.c. injection of 60 mg/kg MCT (Sigma-Aldrich, C-2401) to induce PH. Control animals were injected with the same volume of isotonic NaCl solution. At day 28 after MCT injection, the rats were randomized either to the PIK75 treatment group (50 mg/kg/d) or to the vehicle-treated group.

Su/Hx-induced PH. Male Sprague-Dawley rats (8 weeks old) were s.c. injected with Sugen 5416 (Sigma-Aldrich, S8442) (20 mg/kg dissolved in DMSO) followed by exposure to hypoxia for 3 weeks and normoxia for another 2 weeks (31, 32). Controls received the same amounts of vehicle. Treatment with PIK75 (50 mg/kg/d) or BYL719 (20 mg/kg/d) was carried out during normoxia.

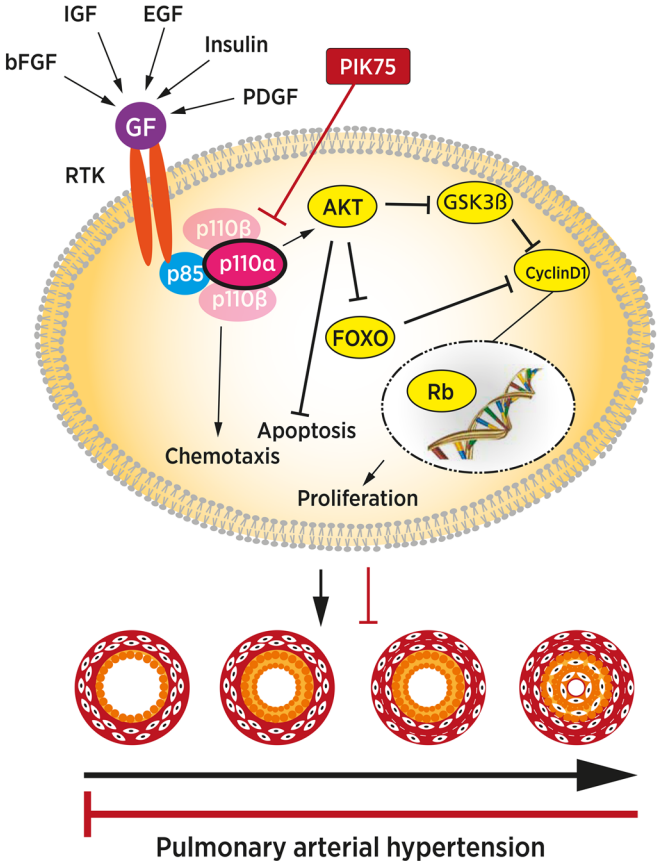

Figure 8. Schematic diagram illustrating a central role for p110α as a therapeutic target in pulmonary hypertension. Several growth factors (GFs) involved in the pathobiology of pulmonary vascular remodeling and pulmonary hypertension (e.g., PDGF, EGF, IGF-I, bFGF) activate their respective RTKs, thereby contributing to PASMC proliferation and chemotaxis and thus inducing vascular remodeling. Class IA PI3K isoform p110α serves as a common downstream target for all of these GFs and is crucial for GF-dependent pathogenic responses of pulmonary arterial smooth muscle cells. Furthermore, p110α is abundantly expressed, and phosphorylation of its downstream target AKT is profoundly enhanced in experimental and human PH. Blunting of p110α action by either a genetic approach or pharmacological inhibition was able to prevent and even reverse pulmonary vascular remodeling, pulmonary hypertension, and right ventricular hypertrophy in various animal models.

Hemodynamic measurements

In mice, hemodynamic analyses were conducted after 21 days of exposure to either hypoxia or normoxia. Accordingly, rats were analyzed after 42 (MCT) or 35 (Su/Hx) days. In mice, anesthesia was realized through a mixture of compressed air (0.6 l/min), oxygen (1–1.2 l/min), and isoflurane (2%). Mice were breathing autonomously through an anesthesia gas–supplying and exhaled gas–dissipating respiratory mask. Rats were anesthetized with a premixed combination of 100 mg/kg ketamine and 4 mg/kg xylazine, tracheostomized, and artificially ventilated. RVSP in mice was determined utilizing a Millar microtip pressure catheter inserted into the RV via the jugular vein. In rats, a fluid-filled catheter was utilized for RVSP measurement. SBP was monitored in the carotid artery. The catheter information was amplified by a PowerLab amplifier and converted to pressure curves using LabChart7 software (AD Instruments).

Assessment of RV hypertrophy

Subsequent to the hemodynamic measurements, the heart was removed, the RV was dissected from the LV and ventricular septum, and wet weight was obtained separately. RV hypertrophy was expressed as the ratio of RV weight to the weight of the LV free wall and ventricular septum (RV/LV + S).

Tissue preparation and morphometric analyses

Lungs were perfused with PBS for 5 minutes, extracted, and fixed in 4% paraformaldehyde. After dehydration, lungs were embedded in paraffin and sectioned into 3 μm sections. Elastica van Gieson staining was performed for determination of the medial wall thickness of pulmonary arteries. Next, α-actin (Sigma-Aldrich, A2547) and vWF (Dako Deutschland GmbH, A0082) double-immunostaining was performed to visualize the smooth muscle layer (purple, Vector Vip. substrate kit, Linaris) of the arteries and the endothelial layer (brown, DAB substrate kit, Linaris) in order to quantify the degree of muscularization of pulmonary arteries. Morphometric analyses were performed using Q Win standard analyzing software (Leica Microsystems GmbH) or QuPath v0.2.0.m-10 open-source software. The degree of muscularization was quantified by half automatic colorimetric/spectrometric detection of the α-actin–positive parts of the vessel wall. The degree of muscularization was defined as follows: nonmuscularized: less than 5%, partially muscularized 5% to 69%, fully muscularized more than 70%. In each animal, more than 80 intraacinar arteries were categorized. In all cases, investigators and slides were blinded for the genotype or treatment group of the respective animals.

BrdU incorporation

DNA synthesis was measured by a BrdU-incorporation assay. Cells were cultured in 96-well plates (1×10^4 cells per well) in DMEM containing 20% FCS for 24 hours or Clonetics SmGm, washed with PBS, and starved in DMEM or Clonetics smooth muscle basal medium (SmBm) for 24 hours. Subsequently, cells were preincubated with inhibitors as indicated for at least 30 minutes followed by growth factor stimulation for 24 hours. BrdU incorporation was carried out according to the manufacturer's specifications (Cell Proliferation ELISA, Roche) with an incubation time of 5 hours as previously described (58). Quantification was performed by measuring the absorbance using Power Wave 340 ELISA reader from Bio-Tek.

Chemotaxis

Growth factor–dependent chemotaxis was assayed utilizing a 48-well modified Boyden chamber (NeuroProbe Inc.) and collagen-coated polycarbonate, PVDF, and filters (8 μm pore size) (GE Water & Process Technologies) as described (58). Briefly, the lower wells of the chamber were filled with DMEM or SmBm supplemented with chemoattractants or vehicle in the presence or absence of inhibitors as indicated. The filters were coated with 50 mg/mL rat type I collagen (BD Biosciences) and fixed atop the bottom wells. Serum-starved SMCs were trypsinized and diluted in DMEM/SmBm to a final concentration of 4×10^5 cells per mL. Where indicated, cells were incubated for 30 minutes with inhibitors and placed into the upper chamber (50 μL per well). The chamber was kept for 5 hours at 37°C in a 5% CO_2 atmosphere and was then disassembled. The cells on the upper surface of

the filter were removed, and the cells on the lower surface were fixed and stained with Diff-Quick (Baxter Healthcare). For quantification, cells were counted using a 20× magnification raster ocular.

Apoptosis

Cell death was determined using Cell Death Detection ELISA (Roche) based on the detection of cytoplasmic histone-associated DNA fragments in apoptotic cells as previously described (59).

Mouse PASMCs. Cells were plated in 96-well plates (1×10^4 cells per well) in DMEM containing 20% FCS for 24 hours followed by serum starvation for 24 hours. Subsequently, cells were stimulated with PDGF-BB (30 ng/mL) or vehicle for 24 hours.

Human PASMCs. Cells were plated in 96-well plates (1×10^4 cells per well) in SmGm for 24 hours followed by application of PIK75 (100 and 300 nM) or vehicle for 24 hours. After collecting the cell lysates (and fixation), the amount of cell death was evaluated using Cell Death Detection ELISA (Roche) according to the manufacturer's specifications. Quantification was performed by measuring the absorbance using Power Wave 340 ELISA reader from Bio-Tek.

Immunoblotting

Quiescent SMCs were left resting or stimulated with growth factors as indicated. Inhibitors were applied 30 minutes before growth factor stimulation. Cells were washed twice with HEPES/sodium chloride (20 mM HEPES, pH 7.4, 150 mM NaCl), and then lysed in extraction buffer (10 mM Tris-HCl, pH 7.4, 5 mM EDTA, 50 mM NaCl, 50 mM NaF, 1% Triton X-100, 0.1% BSA, 20 μg/mL aprotinin, 2 mM Na_3VO_4, 1 mM PMSF). Lysates were centrifuged (20 minutes, 12,000*g*), and the supernatants were subjected to Western blot analysis. Similarly, tissue samples were homogenized in RIPA buffer. Protein concentration was assessed by either the Bradford Assay or NanoDrop quantification. Homogenates were suspended in 4 × SDS sample buffer. Equal amounts of protein lysates were run on SDS–PAGE and transferred to PVDF membranes. Blots were probed with the indicated antibodies.

Immunohistochemistry

Human lung tissue was obtained from either individuals with IPAH or healthy donors undergoing lung transplantation. The study protocol for tissue donation was approved by the Ethics Committee of the University of Giessen (Giessen, Germany) and informed consent was obtained from each patient. Explanted lungs were fixed in 4% phosphate-buffered paraformaldehyde (Santa Cruz Biotechnology). The samples were embedded in paraffin and 3 μm sections were obtained from fixed tissue blocks. Immunohistochemistry was performed using antibodies directed against the phosphorylated human βPDGFR (Abcam, catalog 51046), EGFR (Cell Signaling Technology, catalog 3777), IGFR (Cell Signaling Technology, catalog 3027), and FGFR (Cell Signaling Technology, catalog 9740) with 3,3′-diaminobenzidine as a substrate (DAB Substrate Kit, Linaris). Negative controls were performed with the omission of the primary antibody. Hematoxylin was used to counterstain.

Immunofluorescence staining and assessment of apoptosis and proliferation in vivo

Tissue sections were stained for PCNA (Santa Cruz Biotechnology, sc-7907) to detect proliferation. To assess apoptosis, sections were stained with cleaved caspase 3 (Cell Signaling Technology, 9664S) and visualized using TUNEL with an in situ cell death detection kit (Roche Molecular Biochemicals, 11684795910). Images were counterstained with nuclear DAPI and quantified as described (40).

Real-time qPCR

Total RNA was extracted from human pulmonary artery SMCs using the TRIzol (Life Technologies) RNA extraction method (PMID: 20516177). Equal amounts of isolated RNA were subsequently transcribed into cDNA using high-capacity cDNA reverse transcription kit (Applied Biosystems) according to the manufacturer's instructions. qPCR was then performed with the iQ SYBR Green Supermix (Bio-Rad) kit. Human-specific primers were designed using sequence information from the NCBI database and were purchased from Metabion. Expression was analyzed with the ΔCt method. The Ct values of the target genes were normalized to that of the housekeeping gene (endogenous control) encoding β-2 microglobulin (*B2M*) using the equation $\Delta Ct = Ct_{reference} - Ct_{target}$ and expressed as ΔCt.

Gene name: PDGFRβ; forward primer: ACAATGACTCCCGTGGACTG; reverse primer: CTCGGCATCATTAGGGAGGA; gene name: PDGFβ; forward primer: GAGATGCTGAGTGACCACTCGA; reverse primer: GTCATGTTCAGGTCCAACTCGG; gene name: P110α; forward primer: GAGCATCCATGAAATCTGGTCGC; reverse primer: GAAGCACCTGAATAGGCAAGTCG; gene name: B2M; forward primer: AGATGAGTATGCCTGCCG; reverse primer: TCATCCAATCCAAATGCG.

Materials and antibodies

Chemicals were obtained from Sigma-Aldrich Chemie GmbH. Rat tail collagen type I was obtained from BD Biosciences, elastase from Serva Electrophoresis GmbH, and collagenase from Sigma-Aldrich Chemie GmbH. The antibody against RasGAP (clone 69.3) was a gift from Andrius Kazlauskas (Harvard Medical School). The phospho-Akt Ser473 (catalog 9271), Thr308 (catalog 13038), AKT (catalog 9272), phospho-GSK3β (catalog 9322), GSK3β (catalog 12456), pFoxO 1&3a (catalog 9496), phospho-PDGFRβ (catalog 3161), phospho-Rb (catalog 9308), phospho-tyrosine (catalog 9411), p85 (catalog 4292), p110α (catalog 4255), p110β (catalog 3011), and PCNA (catalog 13110) antibodies were obtained from Cell Signaling Technology; p110δ (catalog 7176), cyclin D1 (catalog 717), and muscle actin (catalog 53141) antibodies from Santa Cruz Biotechnology; and β-actin (catalog ab2827) from Abcam. PDGF-BB (catalog C-63022), bFGF (catalog C-60240), EGF (catalog C-60170), and IGF-I (catalog C-60840) were purchased from Promo Cell. LY-294002 and PIK-75 were from Merck, TGX-221 from Axxora, and IC-87114 from Symansis.

Statistics

All data are expressed as mean ± SEM from at least 3 independent experiments. Statistical analysis was performed using 2-tailed Student's *t* test or 1-way ANOVA and Dunnett's or Newman-Keuls post hoc test as appropriate and as indicated. Statistical significance was defined as $P < 0.05$.

Study approval

Handling and breeding of mice and rats and all experiments were performed in accordance with the German laws for animal protections and were approved by the local animal care committee (Landesamt für Natur, Umwelt und Verbraucherschutz Nordrhein-Westfalen, Reck-

linghausen, Germany) and the Bezirksregierung Köln. For human tissue samples, the study protocol for tissue donation was approved by the Ethics Committee of the University of Giessen in accordance with national law and with Good Clinical Practice/International Conference on Harmonisation guidelines. Written informed consent was obtained from each patient or the patient's next of kin.

Author contributions

EMB conducted experiments, acquired and analyzed data, and wrote the manuscript. CJ, WJ, LLGF, MK, AB, AK, MAA, RS, DWLW, and BP acquired and analyzed data. MV and SB designed research studies and reviewed the manuscript. MZ analyzed data. HTF analyzed data and reviewed the manuscript. SSP provided materials/reagents, acquired and analyzed data, and reviewed the manuscript. JJZ and RTS provided material/reagents and reviewed the manuscript. SR designed research studies, wrote the manuscript, and provided funding.

Acknowledgments

This work was supported in part by the Deutsche Forschungsgemeinschaft (SFB612-B10 to SR and TRR-259 project B06 to SR), the CMMC (project A6 to SR), and the Köln Fortune Program of the Medical Faculty of the University of Cologne (to SR). We thank Andrius Kazlauskas (Harvard Medical School) for providing antibodies against the βPDGFR (clone 97A) and RasGAP (clone 69.3). The technical assistance by Frank Oberhäuser and Maximilian Becker is greatly appreciated. This manuscript contains parts of a doctoral thesis by EMB and MK. EMB was supported by the Graduate Program in Pharmacology and Experimental Therapeutics (Medical Faculty, University of Cologne).

Address correspondence to: Stephan Rosenkranz, Klinik III für Innere Medizin, Herzzentrum der Universität zu Köln, Kerpener Str. 62, 50924 Köln, Germany. Phone: 49.221.478.32356; Email: stephan.rosenkranz@uk-koeln.de.

1. Hoeper MM, et al. A global view of pulmonary hypertension. *Lancet Respir Med*. 2016;4(4):306–322.
2. Galiè N, et al. 2015 ESC/ERS guidelines for the diagnosis and treatment of pulmonary hypertension: the Joint Task Force for the Diagnosis and Treatment of Pulmonary Hypertension of the European Society of Cardiology (ESC) and the European Respiratory Society (ERS): endorsed by: Association for European Paediatric and Congenital Cardiology (AEPC), International Society for Heart and Lung Transplantation (ISHLT). *Eur Heart J*. 2016;37(1):67–119.
3. Humbert M, et al. Pathology and pathobiology of pulmonary hypertension: state of the art and research perspectives. *Eur Respir J*. 2019;53(1):1801887.
4. Schermuly RT, et al. Mechanisms of disease: pulmonary arterial hypertension. *Nat Rev Cardiol*. 2011;8(8):443–455.
5. Hassoun PM, et al. Inflammation, growth factors, and pulmonary vascular remodeling. *J Am Coll Cardiol*. 2009;54(suppl 1):S10–S19.
6. Vonk-Noordegraaf A, et al. Pathophysiology of the right ventricle and of the pulmonary circulation in pulmonary hypertension: an update. *Eur Respir J*. 2019;53(1):1801900.
7. Ryan JJ, et al. Right ventricular adaptation and failure in pulmonary arterial hypertension. *Can J Cardiol*. 2015;31(4):391–406.
8. Reddy S, Bernstein D. Molecular mechanisms of right ventricular failure. *Circulation*. 2015;132(18):1734–1742.
9. Kylhammar D, et al. A comprehensive risk stratification at early follow-up determines prognosis in pulmonary arterial hypertension. *Eur Heart J*. 2018;39(47):4175–4181.
10. Hoeper MM, et al. Mortality in pulmonary arterial hypertension: prediction by the 2015 European pulmonary hypertension guidelines risk stratification model. *Eur Respir J*. 2017;50(2):1700740.
11. Boucly A, et al. Risk assessment, prognosis and guideline implementation in pulmonary arterial hypertension. *Eur Respir J*. 2017;50(2):1700889.
12. Perros F, et al. Platelet-derived growth factor expression and function in idiopathic pulmonary arterial hypertension. *Am J Respir Crit Care Med*. 2008;178(1):81–88.
13. Schermuly RT, et al. Reversal of experimental pulmonary hypertension by PDGF inhibition. *J Clin Invest*. 2005;115(10):2811–2821.
14. Ten Freyhaus H, et al. Genetic ablation of PDGF-dependent signaling pathways abolishes vascular remodeling and experimental pulmonary hypertension. *Arterioscler Thromb Vasc Biol*. 2015;35(5):1236–1245.
15. Ghofrani HA, et al. Imatinib in pulmonary arterial hypertension patients with inadequate response to established therapy. *Am J Respir Crit Care Med*. 2010;182(9):1171–1177.
16. Hoeper MM, et al. Imatinib mesylate as add-on therapy for pulmonary arterial hypertension: results of the randomized IMPRES study. *Circulation*. 2013;127(10):1128–1138.
17. Frost AE, et al. Long-term safety and efficacy of imatinib in pulmonary arterial hypertension. *J Heart Lung Transplant*. 2015;34(11):1366–1375.
18. Merklinger SL, et al. Epidermal growth factor receptor blockade mediates smooth muscle cell apoptosis and improves survival in rats with pulmonary hypertension. *Circulation*. 2005;112(3):423–431.
19. Izikki M, et al. Endothelial-derived FGF2 contributes to the progression of pulmonary hypertension in humans and rodents. *J Clin Invest*. 2009;119(3):512–523.
20. Benisty JI, et al. Elevated basic fibroblast growth factor levels in patients with pulmonary arterial hypertension. *Chest*. 2004;126(4):1255–1261.
21. Dahal BK, et al. Role of epidermal growth factor inhibition in experimental pulmonary hypertension. *Am J Respir Crit Care Med*. 2010;181(2):158–167.
22. Hansmann G, et al. Pulmonary arterial hypertension is linked to insulin resistance and reversed by peroxisome proliferator-activated receptor-gamma activation. *Circulation*. 2007;115(10):1275–1284.
23. Caglayan E, et al. Disruption of platelet-derived growth factor-dependent phosphatidylinositol 3-kinase and phospholipase Cγ 1 activity abolishes vascular smooth muscle cell proliferation and migration and attenuates neointima formation in vivo. *J Am Coll Cardiol*. 2011;57(25):2527–2538.
24. Bilanges B, et al. PI3K isoforms in cell signalling and vesicle trafficking. *Nat Rev Mol Cell Biol*. 2019;9(9):515–534.
25. Thorpe LM, et al. PI3K in cancer: divergent roles of isoforms, modes of activation and therapeutic targeting. *Nat Rev Cancer*. 2015;15(1):7–24.
26. Vanhaesebroeck B, et al. PI3K signalling: the path to discovery and understanding. *Nat Rev Mol Cell Biol*. 2012;13(3):195–203.
27. Manning BD, Toker A. AKT/PKB signaling: navigating the network. *Cell*. 2017;169(3):381–405.
28. Bi L, et al. Proliferative defect and embryonic lethality in mice homozygous for a deletion in the p110alpha subunit of phosphoinositide 3-kinase. *J Biol Chem*. 1999;274(16):10963–10968.
29. Zhao JJ, et al. The p110alpha isoform of PI3K is essential for proper growth factor signaling and oncogenic transformation. *Proc Natl Acad Sci U S A*. 2006;103(44):16296–16300.
30. Vantler M, et al. Class IA phosphatidylinositol 3-kinase isoform p110α mediates vascular remodeling. *Arterioscler Thromb Vasc Biol*. 2015;35(6):1434–1444.
31. Oka M, et al. Rho kinase-mediated vasoconstriction is important in severe occlusive pulmonary arterial hypertension in rats. *Circ Res*. 2007;100(6):923–929.
32. Taraseviciene-Stewart L, et al. Inhibition of the VEGF receptor 2 combined with chronic hypoxia causes cell death-dependent pulmonary endothelial cell proliferation and severe pulmonary hypertension. *FASEB J*. 2001;15(2):427–438.
33. Gurtu V, Michelakis ED. Emerging therapies and future directions in pulmonary arterial hypertension. *Can J Cardiol*. 2015;31(4):489–501.
34. Brachmann SM, et al. Phosphoinositide 3-kinase catalytic subunit deletion and regulatory subunit deletion have opposite effects on insulin sensitivity in mice. *Mol Cell Biol*. 2005;25(5):1596–1607.
35. Geering B, et al. Class IA phosphoinositide 3-kinases are obligate p85-p110 heterodimers. *Proc Natl Acad Sci U S A*. 2007;104(19):7809–7814.
36. Galderisi U, et al. Cell cycle regulation and neural differentiation. *Oncogene*. 2003;22(33):5208–5219.

37. Abid MR, et al. Forkhead transcription factors inhibit vascular smooth muscle cell proliferation and neointimal hyperplasia. *J Biol Chem*. 2005;280(33):29864–29873.
38. Birkenkamp KU, Coffer PJ. Regulation of cell survival and proliferation by the FOXO (Forkhead box, class O) subfamily of Forkhead transcription factors. *Biochem Soc Trans*. 2003;31(Pt 1):292–297.
39. Lam EW, et al. Forkhead box proteins: tuning forks for transcriptional harmony. *Nat Rev Cancer*. 2013;13(7):482–495.
40. Savai R, et al. Pro-proliferative and inflammatory signaling converge on FoxO1 transcription factor in pulmonary hypertension. *Nat Med*. 2014;20(11):1289–1300.
41. Alvarez B, et al. Forkhead transcription factors contribute to execution of the mitotic programme in mammals. *Nature*. 2001;413(6857):744–747.
42. Burgering BMT, Medema RH. Decisions on life and death: FOXO Forkhead transcription factors are in command when PKB/Akt is off duty. *J Leukoc Biol*. 2003;73(6):689–701.
43. Nemenoff RA, et al. Targeted deletion of PTEN in smooth muscle cells results in vascular remodeling and recruitment of progenitor cells through induction of stromal cell-derived factor-1alpha. *Circ Res*. 2008;102(9):1036–1045.
44. Horita H, et al. Selective inactivation of PTEN in smooth muscle cells synergizes with hypoxia to induce severe pulmonary hypertension. *J Am Heart Assoc*. 2013;2(3):e000188.
45. Tang H, et al. Deficiency of Akt1, but not Akt2, attenuates the development of pulmonary hypertension. *Am J Physiol Lung Cell Mol Physiol*. 2015;38(2):L208–L220.
46. Ravi Y, et al. Dysregulation of PTEN in cardiopulmonary vascular remodeling induced by pulmonary hypertension. *Cell Biochem Biophys*. 2013;67(2):363–372.
47. Ten Freyhaus H, et al. Hypoxia enhances platelet-derived growth factor signaling in the pulmonary vasculature by down-regulation of protein tyrosine phosphatases. *Am J Respir Crit Care Med*. 2011;183(8):1092–1102.
48. Lu Z, et al. Loss of cardiac phosphoinositide 3-kinase p110 alpha results in contractile dysfunction. *Circulation*. 2009;120(4):318–325.
49. Sun H, et al. Insulin-like growth factor-1 and PTEN deletion enhance cardiac L-type Ca2+ currents via increased PI3Kalpha/PKB signaling. *Circ Res*. 2006;98(11):1390–1397.
50. Lin RC, et al. PI3K(p110 alpha) protects against myocardial infarction-induced heart failure: identification of PI3K-regulated miRNA and mRNA. *Arterioscler Thromb Vasc Biol*. 2010;30(4):724–732.
51. Workman P, et al. Drugging the PI3 kinome: from chemical tools to drugs in the clinic. *Cancer Res*. 2010;70(6):2146–2157.
52. Rodon J, et al. Development of PI3K inhibitors: lessons learned from early clinical trials. *Nat Rev Clin Oncol*. 2013;10(3):143–153.
53. Chakraboty R, et al. Promoters to study vascular smooth muscle. *Arterioscler Thromb Vasc Biol*. 2019;39(4):603–612.
54. Inuzuka Y, et al. Suppression of phosphoinositide 3-kinase prevents cardiac aging in mice. *Circulation*. 2009;120(17):1695–1703.
55. Foukas LC, et al. Long-term p110α PI3K inactivation exerts a beneficial effect on metabolism. *EMBO Mol Med*. 2013;5(4):563–571.
56. Campa CC, et al. Inhalation of the prodrug PI3K inhibitor CL27c improves lung function in asthma and fibrosis. *Nat Commun*. 2018;9(1):5232.
57. Ray JL, et al. Isolation of vascular smooth muscle cells from a single murine aorta. *Methods Cell Sci*. 2001;23(4):185–188.
58. Rosenkranz S, et al. Identification of the receptor-associated signaling enzymes that are required for platelet-derived growth factor-AA-dependent chemotaxis and DNA synthesis. *J Biol Chem*. 1999;274(40):28335–28343.
59. Vantler M, et al. Systematic evaluation of anti-apoptotic growth factor signaling in vascular smooth muscle cells: only phosphatidylinositol 3′-kinase is important. *J Biol Chem*. 2005;280(14):14168–14176.